Universidade de Brasília
Instituto de Geociências
Programa de Pós-Graduação em Geologia

CARACTERIZAÇÃO DA MINERALIZAÇÃO DE ESTANHO E ÍNDIO DO MACIÇO SUCURI, PROVÍNCIA ESTANÍFERA DE GOIÁS.

Ana Carolina Rodrigues Miranda

Dissertação de Mestrado nº409

Brasília,9 de Março de 2018

Universidade de Brasília
Instituto de Geociências
Programa de Pós-Graduação em Geologia

CARACTERIZAÇÃO DA MINERALIZAÇÃO DE ESTANHO E ÍNDIO DO MACIÇO SUCURI, PROVÍNCIA ESTANÍFERA DE GOIÁS.

Ana Carolina Rodrigues Miranda

Orientador:
Prof. Dr. Nilson Francisquini Botelho

Banca Examinadora:

_____
Prof. Dr. Nilson Francisquini Botelho (UnB)

_____
Profa. Dra. Paola Ferreira Barbosa (UnB)

_____
Prof. Dr. Artur Cezar Bastos Neto (UFRGS)

Brasília, 9 de Março de 2018

À memória de meu

primo-irmão Pedro Felipe

RESUMO

O índio é um componente raro na composição da crosta terrestre. Sua produção mundial tem aumentado constantemente nos últimos anos, devido ao aumento da demanda por aplicações em aparelhos eletrônicos, usinas de energia solar e semicondutores. O índio é encontrado em diversos tipos de depósitos com contribuição magmática e preferencialmente na estrutura de sulfetos de zinco, cobre e estanho, além de óxidos de estanho. Atualmente, 60% da produção de índio é derivada de depósitos vulcanogênicos e sedimentares exalativos. No entanto, depósitos de metais base relacionados a granitos como greisens, stockworks e skarns têm-se tornado cada vez mais atrativos para prospecto de índio. Desde a década de 90 é conhecida a ocorrência de índio na Província Estanífera de Goiás (PEG), associada a granitos estaníferos do tipo A de idade Paleoproterozóica. O Maciço Sucuri (1,77 Ga) é uma pequena intrusão que hospeda mineralização de estanho e índio. Cassiterita é o principal minério de estanho e é hospedada em albitito e greisen juntamente com esfalerita e calcopirita. Dados de química mineral mostram cerca de 0,21 wt.% de índio na cassiterita, 0,45 wt.% na esfalerita e 0,14 wt.% na calcopirita. Além do índio, concentrações relativamente altas de nióbio (2 wt.% de Nb_2O_5) e titânio (1,34 wt.% de TiO_2) foram identificadas na cassiterita. Os cristais de cassiterita apresentam uma zonação oscilatória, com bandas escuras ricas em ferro (0,7 wt.% de FeO) e bandas claras pobre em ferro (<0,1 wt.% de FeO). Os principais mecanismos de entrada de índio na estrutura da cassiterita foram definidos por i. $(Ta,Nb)^{5+} + (Fe,In)^{3+} \leftrightarrow 2Sn^{4+}$, ii. $W^{6+} + 2(Fe,In)^{3+} \leftrightarrow 3Sn^{4+}$ e iii. $(Fe,In)^{3+} + OH^- \leftrightarrow Sn^{4+}. + O^{2-}$. Tanto cristais de esfalerita ricos em índio (0,1 – 0,45 wt.% de In) como os pobres (<0,1 wt.% de In) mostram uma correlação positiva com o Fe sugerindo substituição definida por $In^{3+} + Cu^+ + Fe^{2+} \leftrightarrow 3Zn^{2+}$. Estudos de inclusões fluidas em cassiterita e berilo, de ambas as zonas hidrotermais, identificaram a existência de um sistema puramente aquoso de baixa salinidade (0 a 11,6 wt.% NaCl). Além disso, baixas temperaturas de homogeneização para ambos minerais também foram observadas: 106 a 196 ºC para berilo e 160 a 200 ºC para cassiterita. Tais dados suportam a hipótese de interação de fluidos magmáticos com fluidos meteóricos para a formação do mineralização. Dados de isótopos de enxofre de calcopirita, esfalerita, galena e pirita mostram valores de $\delta^{34}S$ entre -4.86 e -1.52 ‰, os quais se assemelham com enxofre de origem magmática, indicando assim uma fonte mais primitiva para a origem do enxofre. Os resultados apresentados, juntamente com dados da literatura, suportam a existência de dois episódios de mineralização de estanho/índio na Província Estanífera de Goiás (PEG). O primeiro, relacionado à suíte g1, com granitos pouco evoluídos e menos eficiente na concentração de estanho e índio, com

fluidos hidrotermais de baixa temperatura, originando depósitos de pequeno porte, como o do Maciço Sucuri. O segundo episódio está relacionado à suite g2, que envolve granitos altamente evoluídos, com fluidos hidrotermais complexos (H_2O–NaCl–KCl–CO_2), com temperaturas superiores a 300 ºC, que deram origem aos maiores depósitos de estanho e índio da PEG.

Palavras-chaves: Maciço Sucuri, cassiterita, índio, esfalerita, inclusões fluidas, granito tipo A, Província Estanífera de Goiás

ABSTRACT

Indium is a rare element in the composition of the Earth's crust. World production of indium has steadily increased during the last years, because of increased demand for application in electronics, solar power plants and semiconductor. The indium is found in several types of deposits with magmatic contribution and preferentially in the structure of zinc, copper and tin sulfides and tin oxides. Currently, 60% of indium production is derived from volcanogenic and sedimentary exhalation deposits. However, base metal deposits related to granites such as greisens, stockwork, and skarns have become increasingly attractive to indium prospects. Since 1990s, the occurrence of indium in the Goiás Tin Province, Central Brazil, associated with Paleoproterozoic within-plate A-type granites has been known. The Sucuri Massif (1.77 Ga), is a small granitic intrusion that hosts tin and indium mineralization. The petrological characteristics of the intrusion, and mineralization, are similar to other indium occurrences in the province. Two mineralized zones are identified: albitite and greisen. The main occurrence is given by In-bearing cassiterite within the albite. Additionally, disseminated sphalerite, chalcopyrite and helvine group mineral are also with the mineralization. Electron microprobe analyses indicate indium concentrations of up to 0.21 wt.% in cassiterite, 0.45 wt.% in sphalerite and 0.14 wt.% in chalcopyrite. Anomalously values of Nb_2O_5 (i.e. up to 2 wt.%) and TiO_2 (i.e. up to 1.34 wt.%) are also found in cassiterite. Cassiterite crystals are zoned, showing an intercalation of Fe-rich-dark- and Fe-poor-light bands. The main mechanisms for the incorporation of indium within the cassiterite structure are given by i. $(Ta,Nb)^{5+} + (Fe,In)^{3+} \leftrightarrow 2Sn^{4+}$, ii. $W^{6+} + 2(Fe,In)^{3+} \leftrightarrow 3Sn^{4+}$ and iii. $(Fe,In)^{3+} + OH^- \leftrightarrow Sn^{4+}$. Indium-poor (i.e. up to 0.1 wt% In) and In-rich (i.e. 0.1 to 0.45 wt.% In) sphalerites have a positive correlation between Cu and In. This suggests that In and Cu availability within the carrying fluid is an essential control for the In content in sphalerite in hydrothermal systems. Furthermore, a positive correlation between In+Cu and Fe, and a negative correlation between Fe and Zn is also observed. This suggests that the incorporation of In into the sphalerite lattice is given by $In^{3+} + Cu^{+} + Fe^{2+} \leftrightarrow 3Zn^{2+}$. Primary fluid inclusions in cassiterite and beryl indicate that hydrothermal fluids are purely aqueous. Eutetic temperatures vary from -39.9 to -18.3 °C, and support variable concentrations of Na^{+}, K^{+}, Fe^{3+}, Mn^{2+} and Sn^{4+} in the system. Low-salinity and low-homogenization temperatures, indicate a NaCl equiv. below 11 wt.% and crystallization temperatures below 200 ºC. The values of $\delta^{34}S$ in chalcopyrite, sphalerite, galena and pyrite from the albitized granite vary from -4.86 to -1.52 ‰, thus constrained within a magmatic

signature. Petrological, mineralogical, fluid inclusion and isotopic data together with literature data, support the existence of two magmatic mineralizing episodes of Sn and In in the Goiás Tin Province. The first episode is related to g1 suite, which involves less-evolved granite and low-temperature hydrothermal system. This system is responsible for the generation of small tin- and indium- deposits hosted by greisen and albitites, as in the Sucuri Massif. The second episode is related to g2 suite, which involves a highly-evolved granite, with complex hydrothermal fluids (H_2O–NaCl–KCl–CO_2), and a formation temperature above 300 ºC. This suite is responsible for the largest tin- and indium-deposits in the Goiás Tin Province.

Keywords: Sucuri Massif, cassiterite, indium, sphalerite, fluid inclusions, A-type granite, Goiás Tin Province

Lista de Figuras

Lista de Tabelas

Sumário

Capítulo 1 – Introdução

Descoberto em 1863, o índio é um metal relativamente raro, muito utilizado na fabricação de ligas metálicas de baixa temperatura, fotocondutores, baterias e cristais líquidos. Comumente, altas concentrações de índio são encontradas em esfalerita, calcopirita, estanita e cassiterita, dos quais ele é recuperado como subproduto. O índio tem afinidade por depósitos com alguma contribuição magmática ou que indicam componentes de derivação magmática, como depósitos epitermais e do tipo skarn. Os depósitos mais importantes de índio são depósitos de metais base do tipo vulcanogênico e sedimentar exalativo (e.g. cera de 60% da produção mundial), seguido por depósitos associados a plutônicas e/ou vulcânicas calcio-alcalinas a peralcalinas e intermediárias a félsicas (sistemas de veios polimetálicos, stockwork, brechas e greisenização/albitização). Dentre eles destacam-se depósitos de Sn e metais base relacionados a granitos, veios polimetálicos e Cu- porfirítico. Os depósitos relacionados a granito normalmente associado a intrusões rasas (1 a 4 km de profundidade), altamente fracionadas e enriquecidas em elementos litófilos e voláteis como a flúor e o boro, que geralmente hospedam mineralizações de estanho e /ou tungstênio. Dentre eles destacam-se Mount Pleasant, Canadá; Mangabeira, Brasil e Krusné Hory, República Checa.

O Brasil possui importantes reservas estaníferas hospedadas em greisens de idade Proterozóica (Província Estanífera de Goiás; Marini e Botelho, 1986, Províncias Estaníferas de Pitinga e Rondônia; Borges et al., 2009, Bastos Neto et al., 2014; Bettencourt et al., 2016). Desde os anos 90, a ocorrência de índio tem sido investigada somente em um destes depósitos, especificamente na Província Estanífera de Goiás, no Maciço Mangabeira. Neste depósito de estanho e índio, as concentrações são de cerca de 0.3% em peso de In em cassiterita, até 7% em esfalerita e 7% em scorodita, além da presença de minerais de índio, como roquesita ($CuInS_2$), yanomamita ($InAsO_4.2H_2O$) e dzhalindita ($In(OH)_3$). Tais minerais são hospedados em zinnwaldita greisen e em uma rocha formada por quartzo e topázio (Botelho e Moura, 1998; Moura et al., 2007; Moura et al., 2014). Localizado ao sul do maciço Mangabeira, na porção norte da Província Estanífera de Goiás, o maciço Sucuri é um biotita granito que hospeda mineralização de estanho em albititos e greisens. Trabalhos preliminares indicam anomalias de índio associadas a essa mineralização, porém nenhum trabalho de detalhe foi realizado visando à caracterização das rochas e dos minerais portadores desse metal.

Essa dissertação apresenta uma descrição das zonas mineralizadas do Maciço Sucuri, bem como a caracterização litogeoquímica das rochas estéreis e mineralizadas, e um estudo

detalhado dos principais minerais com índio e dos minerais de berílio. Adicionalmente, o trabalho faz a caracterização do fluido hidrotermal e das condições físico-químicas responsáveis pela deposição do minério. Os resultados obtidos são comparados com dados de mineralizações já conhecidas na província e com outros depósitos semelhantes no mundo.

Objetivo e Justificativa

Este trabalho tem por objetivo entender os principais processos que levaram a formação da mineralização de estanho bem como a formação de minerais portadores de índio no Maciço Sucuri. Este objetivo visa responder as seguintes perguntas: i. Quais são os minerais portadores de índio e os principais mecanismos de substituição? ii. Qual a natureza e quais as características do fluido mineralizante? iii. Por que a mineralização de estanho/índio no granito Sucuri possui características distintas das demais mineralizações de estanho observadas na Província?

Visando responder essas perguntas, foram realizadas análises litogeoquímicas, de química mineral em microssonda eletrônica, inclusões fluidas e isótopos estáveis.

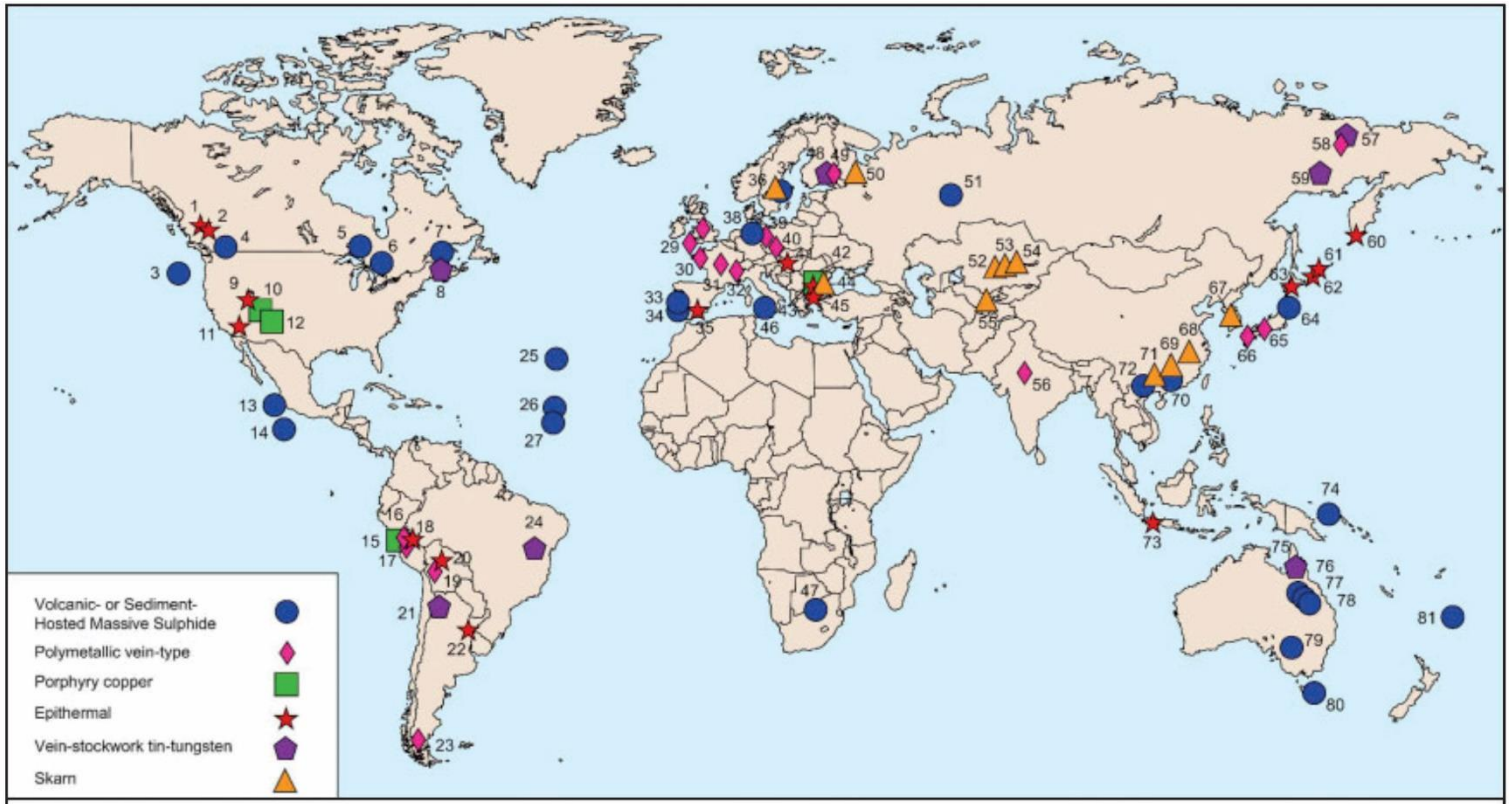

1 Equity Silver	16 Carahuacra	31 Vaulry	46 Palinuro	61 Kudryavy	76 Waterloo
2 Silver Queen	17 Sayapullo	32 Charrier (2 locations)	47 Murchison (2 locations)	62 Prasolov	77 Dry River South
3 Axial seamount	18 Morococha	33 Lagoa Salgada	48 Getmossmalmen (4 locations)	63 Toyoha (8 locations)	78 Balcooma
4 Sullivan	19 Bolivia (9 locations)	34 Neves-Corvo	49 Jungfrubergen	64 Kuroko	79 Broken Hill
5 Geco	20 Malku Khota	35 Cartagena	50 Kitel	65 Akenobe (6 locations)	80 Rosebery
6 Kidd Creek	21 Pirquitas	36 Gåsborn, Bergslagen	51 Southern Urals (6 locations)	66 Kyushu (5 locations)	81 Lau Basin
7 Brunswick Camp	22 San Roque, Rio Negro	37 Långban, Bergslagen	52 Kansay	67 Ulsan	
8 Mount Pleasant	23 Pinguino, Santa Cruz	38 Rammelsberg	53 Kyzyl Espe (4 locations)	68 Qibaoshan	
9 Crypto	24 Mangabeira	39 Freiberg (2 locations)	54 Sarykan (3 locations)	69 Dachang	
10 Bingham	25 Broken Spur	40 Bohemian Massif (7 locations)	55 Karamazar	70 Dachang	
11 McLaughlin	26 TAG, Mid Atlantic Ridge	41 Nagyborzsony	56 Tosham	71 Gejiu	
12 Central District	27 Snake pit	42 Elacite/Asarel, Sredna Gora	57 Deputaskoe	72 Laochang	
13 East Pacific Rise 21°N	28 West Shropshire	43 Sredna Gora (5 locations)	58 Lifudsin	73 Merapi	
14 East Pacific rise 13°N	29 Cornwall (2 locations)	44 Malko-Tarnovo (6 locations)	59 Pravourmiiskoe	74 Manus Basin	
15 Cerro de Pasco	30 Telhaie	45 Kirki	60 Mutnovsky	75 Baal Gammon	

Figura 1a. Distribuição global de depósitos e ocorrências de índio (Schwarz-Schampera, 2014).

Capítulo 2 - Materiais e Métodos

Trabalho de campo foi realizado com o objetivo de coletar amostras de superfície, menos alteradas possíveis, de pontos representativos da mineralização como garimpos e pedreira abandonados. Foram confeccionadas 25 lâminas e 5 secções polidas para análise petrográfica, e 10 amostras entre granitos e minérios foram selecionadas para a litogeoquímica. Todas as análises descritas abaixo foram realizadas nos laboratórios da Universidade de Brasília, com exceção das análises de litogeoquímica que foram encaminhadas para o ACTLABS, utilizando técnicas combinadas de ICP-ES e ICP-MS para elementos principais e menores, respectivamente (pacote 4Litho).

- *Microssonda Eletrônica*

As análises de química mineral em cassiterita, esfalerita e calcopirita foram realizadas por meio da microssonda eletrônica JEOL JXA-8230, com cinco espectrômetros de onda (WDS). Tais análises foram obtidas com aceleração de 20 kV, corrente de feixe de 20nA e diâmetro do feixe de 1 μm. Os tempos de contagem de todos os elementos, com exceção do índio, foram de 10s para cassiterita e de 5s para os sulfetos. O tempo de contagem do índio foi de 60 segundos para cassiterita e de 30 para os sulfetos. Devido às interferências que ocorre entre In e Sn, a calibração do índio foi realizada em uma janela específica para sua detecção, de modo a não ter interferência de Sn. Os picos de Sn-Lα, In-Lα, Nb-Lα foram medidos no cristal de PET, enquanto os picos de Ti-Kα, Fe-Kα, Ta-Lα, W-Lα no cristal LIF. Os limites de detecção dos elementos para cassiterita foram de (em wt.%): 0,02 (In), 0,08 (Nb), 0,02 (Sn), 0,02 (Fe), 0,02 (Ti), 0,02 (Mn), 0,07 (Ta), 0,04 (U), 0,04 (Zn), 0,04 (Pb) e 0,07 (W). Para os sulfetos, os limites de detecção foram (em wt.%): 0,01 (S), 0,02 (In), 0,02 (Ag), 0,04 (Pb), 0,02 (Sn), 0,03 (Zn), 0,02 (Cu), 0,01 (Fe), 0,01 (Cd) e 0,01 (Sb).

Para os minerais do grupo helvita, as análises de química mineral foram realizadas com aceleração de 15 kV e corrente de feixe de 10nA. Os elementos analisados foram Mn, Fe, Zn, Mg, Al, Si, K, Ca, Ti e S. Como o berílio não é analisado diretamente, ele foi calculado estequiometricamente de acordo com Dunn (1976).

- *Inclusões fluidas*

Foram confeccionadas 4 lâminas bipolidas para o estudo de inclusões fluidas em cassiterita e berilo, das principais zonas mineralizadas (albitito e greisen, respectivamente). Os dados microtermométricos foram obtidos utilizando uma platina de resfriamento/aquecimento LINKAM modelo THMSG600, adaptada ao microscópio Olympus BX50 com objetivas de 50x. O equipamento foi calibrado utilizando padrões de inclusões fluidas sintéticas SYN FLINC. A acurácia das medidas variando de ± 0,2°C para resfriamento de até -120°C e para aquecimento até 420°C. Taxas de velocidade em torno de 1°C/min.

- *Isótopos de enxofre*

As análises de isótopos de enxofre foram realizadas em concentrados decalcopirita, galena, pirita e esfalerita usando um espectrômetro de massa Thermo Scientific MAT253 IRMS acoplado ao analisador de elementos Flash 2000. O procedimento consiste em aquecer aproximadamente 2000 μg da amostra de sulfeto para produzir SO_2. Posteriormente, o SO_2 é separado por uma coluna cromatográfica e enviado para ionização. Após a ionização e aceleração da amostra, as espécies de gases com diferentes massas são separadas e analisadas por coletores de faraday. Os resultados são obtidos usando o software Isodat 3.0 e relatados em unidades de por mil (δ34S ‰).

Capítulo 3 – Artigo

Genesis of In-bearing tin mineralization in the Sucuri A-type granite in central Brazil: evidence from In-bearing minerals, beryllium minerals, fluid inclusions and sulfur isotope data.

Ana Carolina Rodrigues Miranda, Nilson Francisquini Botelho

Universidade de Brasília, Instituto de Geociências, Brasília, DF 70910-900, Brazil

Abstract

Indium-tin mineralization in the Goiás Tin Province, Central Brazil, is restricted to Paleoproterozoic within-plate A-type granites. Based on petrological features, these granites are divided in two suites, g1 and g2. The g2 suite is younger and more evolved than g1 and is responsible for the formation of significant tin and indium deposits. The g1 Sucuri Massif (1.77 Ga) is a small granitic intrusion that hosts tin and indium mineralization. Two mineralized zones are identified: greisen and albitite. The main occurrence consists of In-bearing cassiterite within the albitite. Additionally, disseminated sphalerite, chalcopyrite and helvine group minerals are found with the mineralized zones. Electron microprobe analyses indicate indium concentrations of up to 0.21 wt.% in cassiterite, 0.45 wt.% in sphalerite and 0.14 wt.% in chalcopyrite. Anomalous values of Nb_2O_5 (*i.e.*, up to 2 wt.%) and TiO_2 (*i.e.*, up to 1.34 wt.%) are also found in cassiterite. Cassiterite crystals are zoned, showing an intercalation of Fe-rich dark and Fe-poor light bands. The main mechanisms for the incorporation of indium within the cassiterite structure are given by i. $(Ta,Nb)^{5+} + (Fe,In)^{3+} \leftrightarrow 2Sn^{4+}$, ii. $W^{6+} + 2(Fe,In)^{3+} \leftrightarrow 3Sn^{4+}$ and iii. $(Fe,In)^{3+} + OH^- \leftrightarrow Sn^{4+}$. Indium-poor (*i.e.*, up to 0.1 wt% In) and In-rich (*i.e.*, 0.1 to 0.45 wt.% In) sphalerites have positive correlations between Cu and In. This result suggests that In and Cu availability within the carrying fluid is an essential control for the In content in sphalerite in hydrothermal systems. Furthermore, a positive correlation between In+Cu and Fe and a negative correlation between Fe and Zn are also observed. These results suggest that the incorporation of In into the sphalerite lattice is given by $In^{3+} + Cu^{+} + Fe^{2+} \leftrightarrow 3Zn^{2+}$. The occurrence of helvine group minerals associated with beryl and phenakite in the mineralized rocks constrains their formation to very limited intervals for $f(S_2)$ and $f(O_2)$ (*i.e.*, pyrrhotite domain). Primary fluid inclusions in cassiterite and beryl indicate that the hydrothermal fluids are purely aqueous. Final ice melting temperatures vary from -39.9 to -18.3°C and support

variable concentrations of Na^+, K^+, Fe^{3+} and Mn^{2+} in the system. Low salinities and low homogenization temperatures indicate an NaCl equiv. below 11 wt.% and crystallization temperatures below 200ºC. The values of $\delta^{34}S$ in chalcopyrite, sphalerite, galena and pyrite from the albitized granite vary from -4.86 to -1.52‰ and are thus constrained within a magmatic signature. Petrological, mineralogical, fluid inclusion and isotopic data, together with data from the literature, support the existence of two magmatic mineralizing episodes for Sn and In in the Goiás Tin Province. The first episode is related to the g1 suite, which involves less evolved granite and a low-salinity and low-temperature hydrothermal system. This system is responsible for the generation of minor In-bearing tin deposits, such as the Sucuri area, hosted by albitites and greisen veins. The second episode is related to the emplacement of the g2 suite. This system involves a highly evolved granite with major tin-indium deposits in greisenized cupolas generated by complex hydrothermal fluids (H_2O–NaCl–KCl–CO_2) with temperatures above 300ºC.

Keywords: Cassiterite, indium, sphalerite, helvine group, fluid inclusions, Sucuri A-type granite, Brazil

1. Introduction

Indium was discovered by Ferdinand Reich and Hieronymus Richter in 1863 during the study of a polymetallic vein-type zinc deposit from Freiberg district, Erzgebirge (Germany). Therefore, it is a chalcophile and relatively rare element that occurs in trace concentrations in zinc, copper and tin sulfides. Due to its characteristics (soft, silver-white and highly malleable and ductile metal), indium has wide applicability, including in semiconductors, solar cells, batteries, liquid crystal displays and low-temperature solders (Schwartz-Schampera & Herzig, 2002). Although twelve indium minerals are described (Picot & Pierrot, 1963, Ohta 1980, Genkin & Murav'eva 1963, Razin *et al.* 1981, Kissin & Owens 1989, Kato 1965, Botelho *et al.* 1994, Ivanov 1963, Yu *et al.* 1974 and Mandarino 1996), indium is extracted as by-product only from Zn, Sn and Cu deposits (Werner *et al.* 2017). These deposits include diverse geological settings such as volcanic- and sediment-hosted exhalative massive sulfide, epithermal, polymetallic base metal vein, granite-related tin-base metal and skarn deposits (Schwartz-Schampera & Herzig 2002).

Volcanic- and sediment-hosted massive sulfide (VMS and SEDEX) deposits represent more than 60% of In resources (Werner *et al.* 2017). Additionally, indium is reported in granite-

related tin-base metal deposits, including skarn-, greisen-, and vein-type mineralizations including Mount Pleasant (Sinclair *et al.* 2006), Finland (Cook *et al.* 2011c, Valkama *et al.* 2016), Erzgebirge (Seifert 2008, Seifert *et al.* 2015), Mangabeira (Moura *et al.* 2014), Far East Russia (Pavlova *et al.* 2015) and SW England (Andersen *et al.* 2016). In these cases, indium is associated with highly fractionated granitic intrusions enriched in lithophile elements and volatiles such as boron and fluorite (Schwartz-Schampera & Herzig, 2002). Therefore, these highly fractionated granitic intrusions are important exploration targets for indium.

In Brazil, the existence of Sn-polymetallic deposits related to Proterozoic within-plate granitic intrusions has been extensively documented: the Pitinga Tin Province and Rondônia Tin Province in the Amazon region (Bettencourt *et al.* 2005, 2016, Borges *et al.* 2009, Bastos Neto *et al.* 2014) and the Goiás Tin Province (GTP) in central Brazil (Botelho & Moura, 1998). However, the occurrence of indium has been reported only in the GTP, which is represented by the presence of indium- and indium-bearing minerals within cassiterite-dominated deposits, with measured reserves of 27000 t of Sn (Bettencourt 1997, Botelho & Moura 1998, Moura *et al.* 2014).

The Sucuri Massif is a small tin deposit that contains indium-bearing minerals. The occurrence of some indium-bearing minerals in this massif is similar to that reported in the nearby Mangabeira tin deposit by Botelho and Moura (1998). Therefore, the Sucuri area may represent a future target for In exploration. In this work, we provide a detailed characterization of the distribution of rare metals and indium in cassiterite and sulfides (*i.e.*, sphalerite and chalcopyrite) from the Sucuri Massif. In addition, petrological, fluid inclusion and isotopic analyses also support a discussion about the origin of indium occurrences within the Sucuri Massif and Goiás Tin Province.

2. Regional setting

The Goiás Tin Province, located in the Neoproterozoic Brasília Fold Belt, Tocantins Province, comprises a wide region in Goiás State that hosts tin deposits related to Paleo- to Neoproterozoic granitic intrusions. It is divided in four subprovinces according to their location: Rio Tocantins, Rio Paranã, Goianésia-Pirenópolis and Ipameri (Marini and Botelho, 1986). The two most important subprovinces, Rio Tocantins (RTS) and Rio Paranã (RPS), are located in the northern portion of the state (Fig. 1a) and host extensive tin deposits associated with within-plate A-type granites. The within-plate granites are divided into two suites according to

petrological, geochemical, geochronological and metallogenetic characteristics (Botelho 1992): (i) the 1.77 Ga g1 granites and (ii) the 1.6-1.5 Ga g2 granites (U-Pb ages, Pimentel *et al.* 1999). Both suites have high F, Sn, Rb, Y, Th, Nb, Ga and REE contents. Nb/Ta ratios greater than 1 and high F/Li ratios allow their classification as rare-metal granites of NYF (for Nb, Y, F: Cerny 1991). The g1 suite is less evolved and more potassic, with alkaline affinity and high Nb, Zr, Th, Y and REE contents. It is part of the rapakivi magmatic suite in central Brazil (Lenharo *et al.* 2002). The g2 suite is metaluminous to peraluminous and highly evolved with lower K/Na ratios and higher Li, Rb, Sn and Ta contents and hosts tin mineralization (Botelho 1992, Lenharo *et al.* 2002, Moura *et al.* 2014). Both suites were generated either by melting of a heterogeneous Archean–Paleoproterozoic crust or by different degrees of mixing between mafic and felsic magmas with predominant crustal components (Lenharo *et al.* 2002).

The 1.77 Ga Sucuri Massif (RPS, Fig, 1a) is a biotite-bearing granite that covers an area of approximately 8 km². It is texturally divided into four facies (Bilal *et al.* 1997): i) medium grained, which is the most abundant, ii) fine grained, iii) fine grained porphyritic and iv) microgranitic (Fig. 1b). The mineralogy is composed of quartz, microcline (eventually perthitic), plagioclase (sodic oligoclase to albite) and biotite. The accessory minerals zircon, monazite, apatite, ilmenite and fluorite are generally more abundant in the fine-grained facies (Bilal 1991, Bilal *et al.* 1997). Tin mineralization at Sucuri occurs mainly in the hydrothermal albitites, greisen and quartz veins, controlled by fracture zones with directions N60°W and N40°W. Cassiterite is the only tin ore. Major sphalerite and chalcopyrite and minor galena, pyrite, pyrrhotite and cubanite are also present. Greisen and quartz veins occur in the apical part associated with the fine-grained facies (*e.g.*, Garimpo Vaca Velha; Fig. 1b). Albitites occur in the southern and northeastern parts of the intrusion, next to Garimpo dos Cachorros and Tratex Quarry (Fig. 1b), associated with medium-grained biotite granite. The albitization overprints the original foliation of the medium-grained facies and the greisenized zones (Bilal *et al.*1997).

2.1 Indium-bearing tin ore in the Goiás Tin Province

Vein-stockwork deposits of tin and tungsten occur in a wide variety of structural styles (individual or multiple vein systems, breccias and replacement zones in altered wall rocks). These deposits generally occur in or near highly fractionated granitic intrusions, which have

been emplaced at relatively shallow levels (1 to 4 km) in the crust. Such intrusions are typically enriched in rubidium, lithium, beryllium, tin, tungsten, tantalum, niobium, thorium and rare earth elements, as well as in volatile elements such as fluorite and boron. These characteristics make such deposits important hosts for indium mineralization (Schwartz-Schampera & Herzig 2002, Sinclair *et al.* 2006).

In the Goiás Tin Province, the Mangabeira Massif hosts an important tin-indium mineralization (Fig. 1a) closely associated with evolved biotite granite and topaz albite granite (g2 suite, Botelho & Roger 1990, Botelho *et al.* 1994, Moura *et al.* 2007, 2014). Cassiterite and minor wolframite are the main ore minerals. Indium-bearing sulfides, arsenates and cassiterite are hosted in Li-bearing phengite–quartz greisen and topaz–zinnwaldite greisen. The main indium carriers are scorodite ($FeAsO_4 \cdot 2H_2O$) (up to 7 wt.% In_2O_3), sphalerite (up to 6.7 wt.% In), yanomamite ($InAsO_4 \cdot 2H_2O$), roquesite ($InFeS_2$) and dzhalindite ($In(OH)_3$). Minor indium concentrations are found in cassiterite (up to 0.3 wt.% In_2O_3), chalcopyrite (up to 0.23 wt.% In), digenite (up to 0.11 wt.% In) and arsenopyrite (up to 0.3 wt.%) (Botelho 1992, Botelho *et al.* 1994, Botelho & Moura 1998, Moura 1993, Moura *et al.* 2007).

Indium concentrations in the province are probably related to fluorite-rich post-magmatic/hydrothermal alteration, favoring the transport of Sn and In and the precipitation of In-rich cassiterite (Moura *et al.* 2014). Previous studies show that as well as the Mangabeira deposit, others granitic bodies (*i.e.,* Sucuri and Pedra Branca massifs) also contain significant In-bearing minerals (*i.e.*, cassiterite, sphalerite, stannite and chalcopyrite) associated with tin mineralization. Hence, the investigations of these In-bearing minerals may have an economic impact on tin exploration in this region (Botelho *et al.* 1994, 1998), and this work investigates, for the first time, the mineralogy and geochemistry of this metal in the Sucuri Massif.

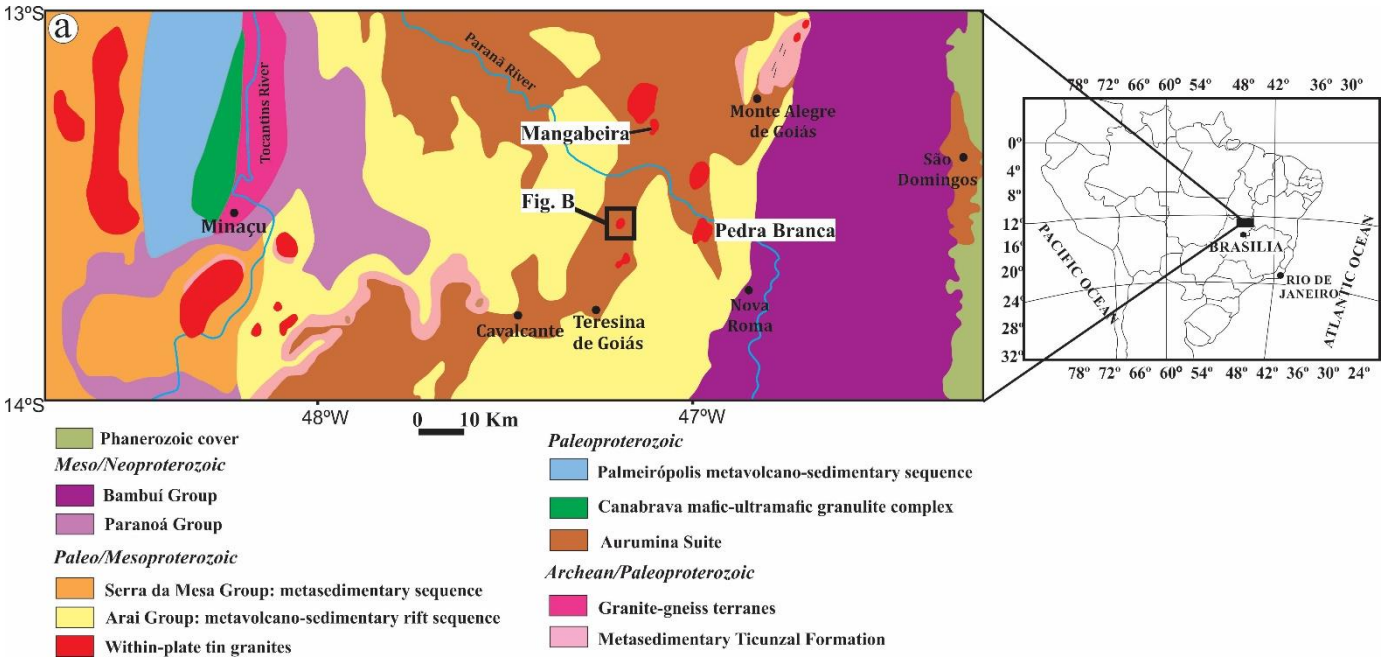

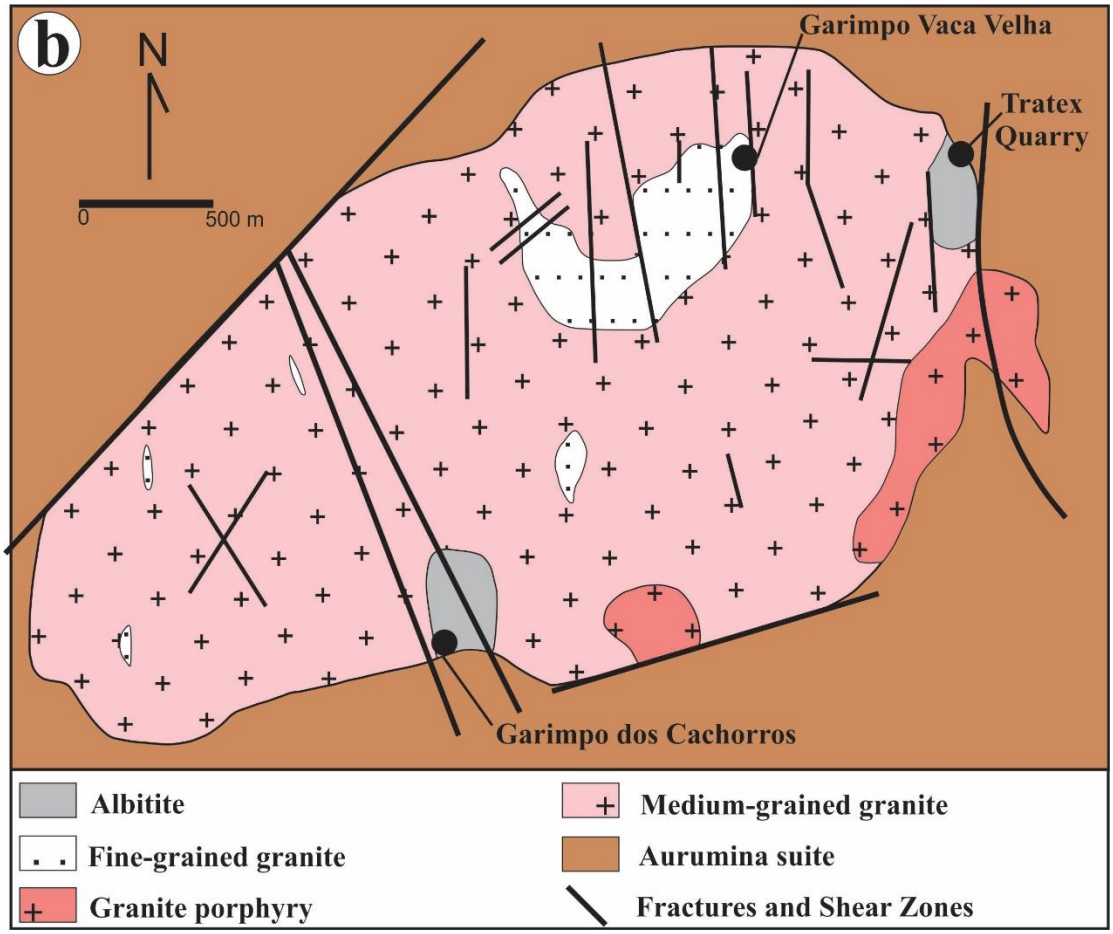

Figure 1. (a) Geological map of the northern portion of the Goiás Tin Province, with location of the Sucuri, Mangabeira and Pedra Branca massifs (RPS). In the western side is located massifs from Rio Tocantins Province and the east massifs from Rio Paranã Province. (b)

Geological map of the Sucuri Massif and location of quarry and garimpos (adapted from Bilal, 1991).

3. Analytical methods

For this study, outcrops from mineralized and barren zones were systematically sampled in order to select unweathered rocks. All analyses described below were performed in laboratories at the University of Brasília, except the lithogeochemical analyses (10 samples), which were performed at ACTLABS, Canada, using combined techniques of ICP-ES and ICP-MS for major and minor elements, respectively (4 Litho package).

Mineral analyses were performed on polished thin sections using a JEOL JXA-8230 SuperProbe with five wavelength dispersive spectrometers (WDS). These analyses were obtained for cassiterite, sphalerite and chalcopyrite, with an accelerating voltage of 20 kV, a beam current of 20 nA and a probe diameter of 1 µm. The counting times for all elements except indium on background and peak were 10 s and 5 s, respectively. For indium analyses, the counting times in cassiterite and sulfides were 60 s and 30 s, respectively. Indium analyses in tin-rich minerals by EMPA must be carefully conducted due to the interferences between In and Sn (Schwartz Schampera & Herzig, 2002). Therefore, the In calibration was performed in a window for the detection of the In-peak without Sn interference. The Sn-*L*α, In-*L*α, and Nb-*L*α peaks were measured in the PET crystal, while the Ti-*K*α, Fe-*K*α, Ta-*L*α, and W-*L*α peaks were measured in the LIF crystal. The detection limits of the elements for cassiterite were (in wt.%) 0.02 (In), 0.08 (Nb), 0.02 (Sn), 0.02 (Fe), 0.02 (Ti), 0.02 (Mn), 0.07 (Ta), 0.04 (U), 0.04 (Zn), 0.04 (Pb) and 0.07 (W). For sulfides, the detection limits were (in wt.%) 0.01 (S), 0.02 (In), 0.02 (Ag), 0.04 (Pb), 0.02 (Sn), 0.03 (Zn), 0.02 (Cu), 0.01 (Fe), 0.01 (Cd) and 0.01 (Sb). Pavlova *et al.* (2015) compared EMPA analyses with a similar calibration and LA-ICP-MS analyses of cassiterite with variable concentrations of In, and the results showed an excellent correlation. For helvine group minerals, EMPA analyses were carried out with an accelerating voltage of 15 kV and a beam current of 10 nA. The analyzed elements were Mn, Fe, Zn, Mg, Al, Si, K, Ca, Ti and S. Beryllium was not directly analyzed and was stoichiometrically calculated following Dunn (1976).

Fluid inclusions hosted in beryl and cassiterite crystals from greisen and albitite samples were characterized using double-polished thin sections. Microthermometric data were obtained using a LINKAM THMSG600 heating-freezing stage attached to a petrographic microscope OLYMPUS BX50 with an objective of 50x. The heating-freezing stage was calibrated using

the SYN FLINC synthetic standards, applying speed rates of 1°C/min and an estimated accuracy of ± 0.2ºC for the freezing stage (*i.e.*, from 25º to -120ºC) and ± 2ºC for the heating stage (*i.e.*, up to 420ºC).

Sulfur isotope analyses were performed in chalcopyrite, galena, pyrite and sphalerite using a Thermo Scientific MAT253 IRMS mass spectrometer coupled to a Flash 2000 element analyzer. The procedure consisted of heating approximately 2000 µg of sulfide grains to approximately 1800ºC to produce SO_2. Subsequently, the SO_2 was separated by a chromatographic column and then sent to the ion fount for ionization. After the ionization and acceleration of the sample, gas species with different masses were separated and analyzed by Faraday cup collectors. The results were obtained using the software Isodat 3.0 and reported in units of per mil ($\delta^{34}S‰$).

4. Indium-bearing tin mineralization

4.1 Geology and Textural relationship

The Sucuri Massif is a within-plate granite that hosts tin mineralization. It is intrusive into Paleoproterozoic granite gneiss of the Aurumina Suite. The tin mineralization is mainly hosted by two hydrothermal facies: greisen and albitite. Greisen is more restricted than albitite and occurs only at the apical part of the intrusion (Garimpo Vaca Velha, Fig. 1b). This facies occurs locally associated with quartz veins. Albitites are observed in two distinct regions, but only one of them hosts tin mineralization (Fig. 1b; Garimpo dos Cachorros). The albitization process is late than the greisenization, whereas the greisen is slightly albitized (Bilal 1991). The mineral assemblages of the biotite granite and hydrothermalized zones are summarized in Table 1.

The most extensive facies of the Sucuri massif is a medium-grained biotite granite with gray coloration and syn-magmatic foliation (Fig. 2a). According to Bilal (1991) and Bilal *et al.* (1997), the Sucuri Massif is intruded by a fine-grained granite with a higher concentration of albite and lower concentration of quartz. These late intrusions are locally responsible for the muscovitization of the medium-grained granite and by formation of the greisens and quartz veins. The hydrothermal mineral assemblage developed during greisenization includes quartz, muscovite (Fig. 2b) and variable amounts of cassiterite, phenakite, fluorapatite, biotite, fluorite and beryl. Locally, small grains of a bismuth-bearing mineral (*i.e.*, up to 100 um) are observed

in the matrix. Garnet (spessartine) and phenakite are also present, commonly associated with helvine (Fig. 2b).

Different stages of albitization are observed in the vicinity of the ore. This alteration overprints the magmatic texture of the granite, giving rise to a white-colored and anisotropic rock (Fig. 2c). Two albitized zones are individualized in the Sucuri massif: (i) a tin-mineralized zone with 60-70% cassiterite (Fig. 2d) located in the Garimpo dos Cachorros and (ii) barren albitite in the Tratex Quarry (Fig. 1b). The evolution of the hydrothermal alteration is traced by a decrease in the silica content and the replacement of microcline (perthite) by albite (Fig. 2e). In addition to albite, the hydrothermal mineral assemblage contains cassiterite, sulfides (*i.e.*, sphalerite, chalcopyrite, galena, pyrite and minor pyrrhotite and cubanite), fluorite, helvine group minerals, ilmenite and apatite.

Apart from albitites, hydrothermally altered rocks with partially preserved primary textures are also observed and classified as albitized granite. These rocks show relicts of the primary mineralogy of the medium-grained granite (i.e., quartz, microcline, plagioclase and biotite), with slight albitization. In this case, microcline is partially replaced by albite (Fig. 2f), and this rock shows variable amounts of disseminated sulfides and cassiterite. Locally, small quartz-cassiterite veinlets are observed in all hydrothermalized facies. Finally, the medium-grained granite and the hydrothermalized rocks exhibit an incipient late alteration. In this case, minerals such as microcline, biotite and chalcopyrite are replaced by muscovite, chlorite and covellite, respectively.

Table 1. Different mineralogical assemblages observed in the biotite granite, greisen and albitite of the Sucuri Massif.

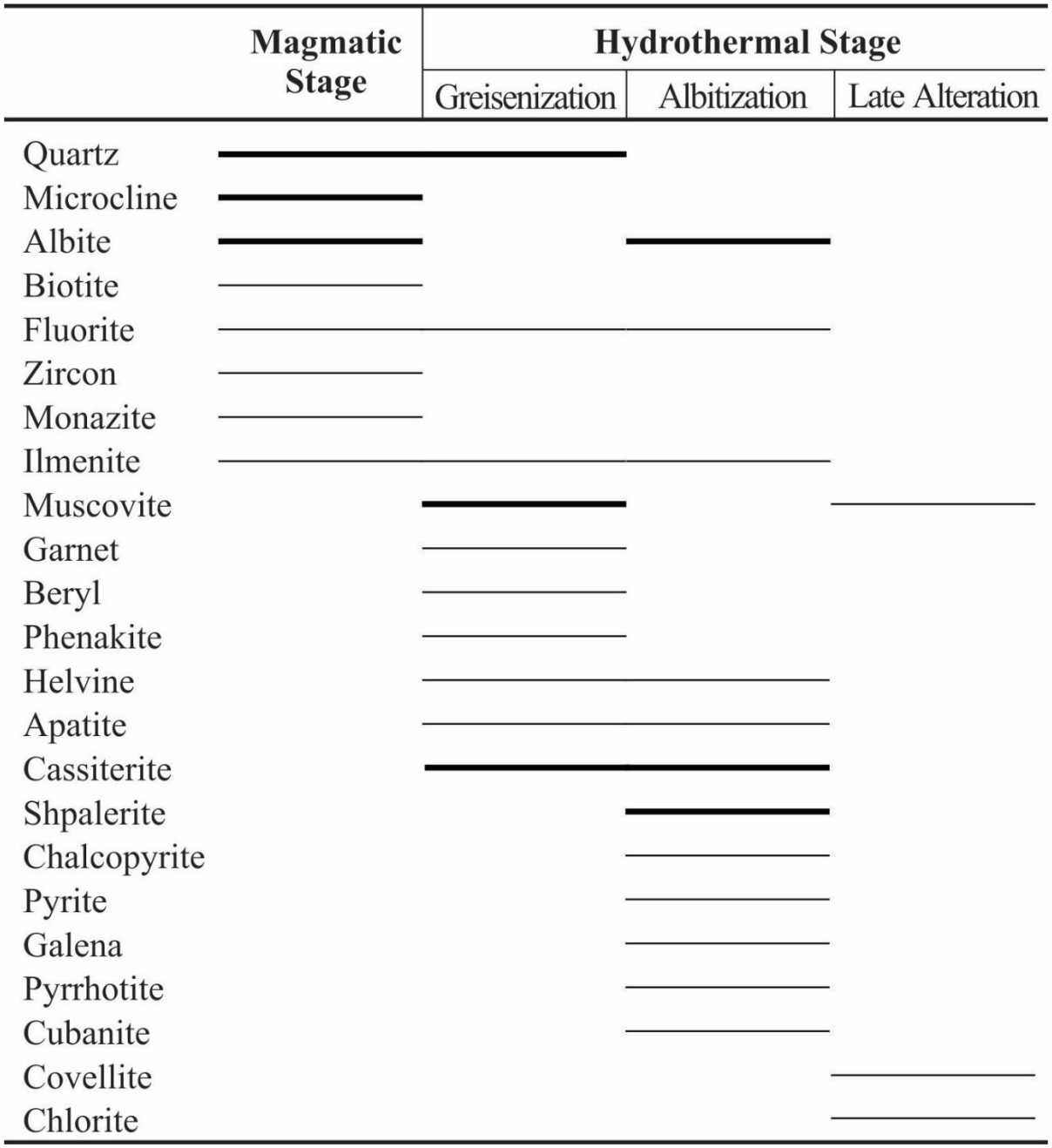

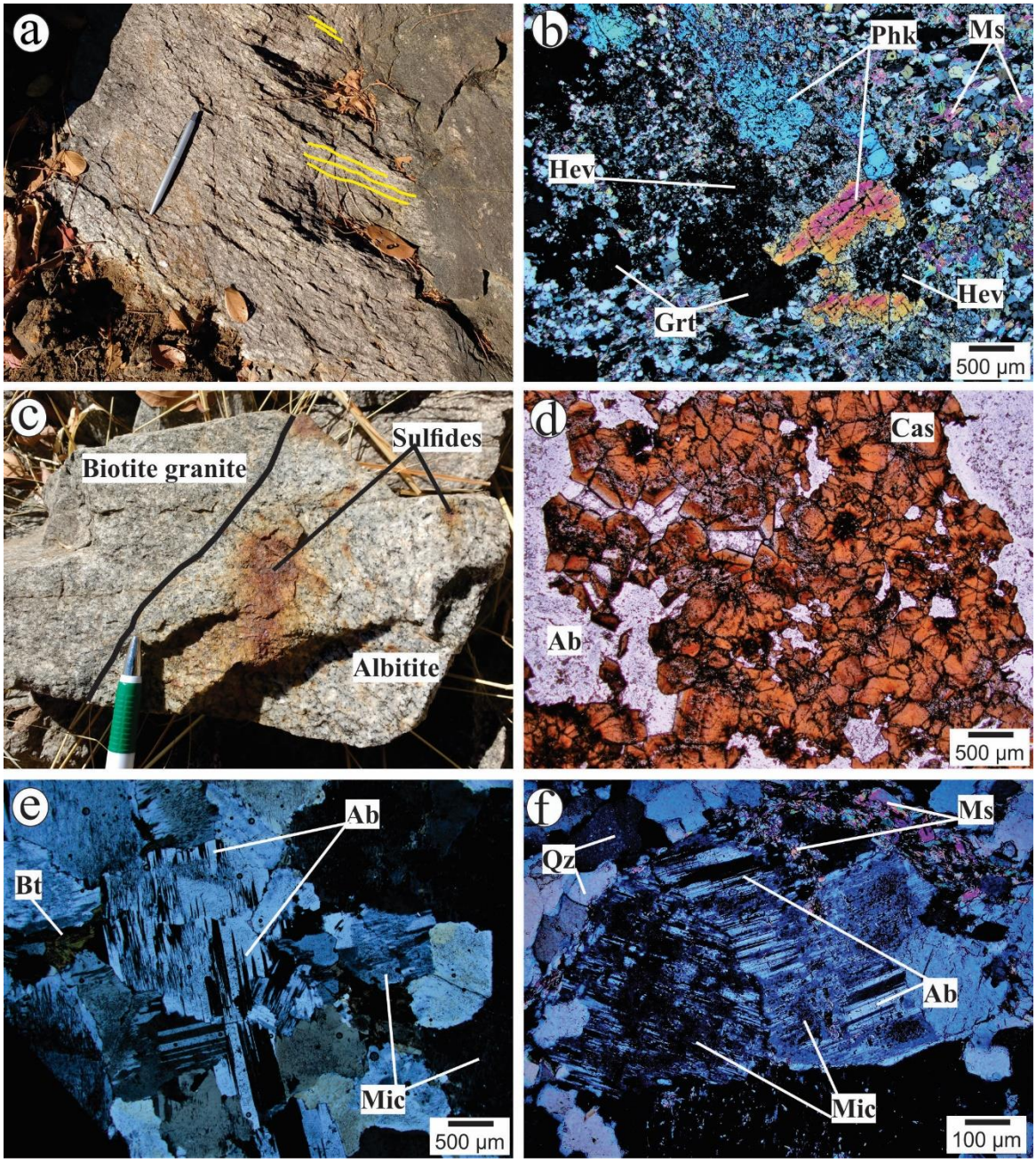

Figure 2. Photographs and photomicrographs of representative unaltered granite and hydrothermal rocks of the Sucuri massif. (a) Outcrop of medium-grained biotite granite with mylonitic foliation (highlighted by the yellow lines); (b) Photomicrograph of greisen showing textural relationship between garnet, phenakite and helvine inserted in fine quartz-muscovite groundmass. Garnet and phenakite grains are not in equilibrium with helvine grains; (c) Hand specimen showing the changes in texture and color between medium-grained biotite granite to albitite. Note the difference between the texture from figure 2a. (d) Photomicrograph of mineralized albitite showing textural relationship between zoned and homogenous cassiterite and albite. (e) Photomicrograph of albitite exhibiting advanced albitization in microcline crystals. (f) Photomicrograph of albitized granite. Note the relicts of perthitic microcline being replaced by hydrothermal albite and the relicts of quartz grains. Fine muscovite lamellae are replacing microline crystals. Abbreviations Ab: albite; Bt: biotite; Cas: cassiterite; Grt: garnet; Hev: helvine; Mic: microcline; Ms: muscovite; Phk: phenakite; Qz: quartz.

4.2 Bulk ore geochemistry

A group of ten representative samples of the fine-grained granite and hydrothermalized zones from the Sucuri Massif were selected for the geochemical investigation. The results are given in Table 2. Tin-mineralized rocks, also including albitized granites in the vicinity of the ore (*i.e.,* analyses 4 and 5), contain more than 500 ppm Sn (Table 2). These concentrations are up to 10 times greater than those from the fine-grained biotite granite (*i.e.,* 50 ppm Sn; Table 2, analysis 1). In addition, indium concentrations in these rocks vary from 4.5 to 75.5 ppm. The highest In contents (*i.e.,* 49.4 and 75.5 ppm), above the greisen, are from rocks with more than 1 wt.% Zn (Table 2, analyses 7 and 8). In Sn-rich samples (*i.e.,* Table 2, analyses 5, 9 and 10), the indium concentrations do not exceed 42.6 ppm. High values of Nb (*i.e.,* up to 3990 ppm) and W (i.e., up to 951 ppm) are associated with high concentrations of Sn (*i.e.,* > 10 wt.% Sn; Table 2, analyses 9 and 10).

Indium shows positive correlations with Zn and Cu (Fig. 3a and 3b, respectively). In addition, a negative correlation between In and Sn is observed (Fig. 3c). Niobium and Sn (Fig. 3d) and Cu and Zn (Fig. 3e) also show positive correlations. In general, both the g1 and g2 suites from the Goiás Tin Province are characterized by distinct Ta/Nb ratios (Botelho & Moura 1998). The g2 suite has a Ta/Nb ratio >0.23, whereas this ratio in the g1 suite is approximately 0.1. Such values suggest that mineralized zones from the Sucuri Massif are associated with the g1 suite (Fig. 3f).

Table 2. Whole-rock analyses of indium-tin-mineralized zones from the Sucuri Massif.

	Biotite granite	Albitized granite				Barren albitite	Albitite mineralized			Greisen
Sample	1	2	3	4	5	6	7	8	9	10
SiO2 (%)	71,81	66,73	67,15	68,29	59,92	64,62	60,53	78,41	17,29	40,23
TiO2	0,182	0,263	0,184	0,155	0,013	0,17	0,214	0,013	0,703	0,163
Al2O3	13,47	16,56	14,7	15,32	15,91	18,45	16,84	10,54	5,56	3,51
Fe2O3	2,66	2,73	3,9	2,18	0,29	4,35	4,54	0,81	0,58	1,83
MnO	0,041	0,035	0,028	0,028	0,008	0,168	0,081	0,016	0,034	0,109
MgO	0,09	0,08	0,06	0,05	<0.01	0,12	0,11	0,02	0,03	0,04
CaO	0,69	0,23	1,54	0,83	0,07	0,98	3,33	0,3	0,34	0,55
Na2O	2,97	5,73	4,84	4,31	4,22	9,94	7,25	5,16	2,92	1,06
K2O	5,48	5,68	5,71	6,06	6,56	0,36	1,53	0,48	0,28	0,72
P2O5	0,06	0,09	0,08	0,05	0,04	0,08	0,06	0,12	0,03	0,16
LOI	1,17	1,13	1,82	1,27	0,61	0,61	2,44	0,82	0,46	0,53
Total	98,62	99,26	100	98,54	87,65	99,84	96,92	96,7	28,21	48,89
Be	12	12	6	34	3	669	279	9	28	917
Rb	698	376	352	484	561	89	337	77	39	304
Cs	5,3	0,6	0,5	1,5	1,2	3,4	4,4	<0.5	0,8	14,2
Ba	165	433	384	220	28	40	125	38	21	62
Sr	23	56	51	36	11	70	80	24	10	70
Ga	41	33	28	30	32	30	32	24	18	18
V	5	8	5	5	5	8	7	<5	63	6
Sn	50	43	138	686	77270*	34	3867*	599	537950*	229260*
In	**<0.2**	**<0.2**	**<0.2**	**15,2**	**4,5**	**0,9**	**49,4**	**75,5**	**29,5**	**42,6**
W	10	4	4	7	95	1	11	5	951	380
Ta	12,3	14,9	10,4	7,9	7	8,6	9,3	0,6	67,3	93,6
Nb	112	119	104	72	33	81	99	7	3990*	620
Th	98,8	78,9	68,1	49,7	25,3	58,8	52,9	46,1	12,3	1,2
U	18,7	22,5	18,4	15	10,7	17,4	12,9	3,1	15,1	27
Zr	292	285	261	155	50	226	200	137	327	154
Hf	10,9	9,9	9	5,2	3,2	7,8	6,8	4,1	42,1	33,3
Y	200	141	85	106	58	119	116	30	13	31
Sc	7	6	5	3	4	9	4	2	155	60
Co	< 1	3	4	1	<1	3	2	2	4	3
Cu	< 10	50	330	4230	10	50	3550	280	30	30
Zn	100	<30	100	580	<30	2980	14603*	19470*	1250	740
Pb	31	55	413	29	37	76	2540	76	397	44
Bi	< 0.4	0,7	3,7	< 0.4	0,7	0,6	4,8	0,4	1,4	6,7
La	197	128	151	101	34,4	113	109	102	28,6	13,6
Ce	397	257	284	203	81,7	228	219	207	57,6	22
Pr	43,1	28,2	30,3	22	9,41	25,4	24,5	22,5	6,35	2,34
Nd	145	96	96,7	76,4	31,5	85,5	83,8	78,1	22,2	7,4
Sm	32,9	22,4	18,2	16,7	9,6	19,9	20,4	15,6	4,8	2
Eu	0,57	0,56	0,38	0,44	0,08	0,47	0,57	0,22	0,11	0,19
Gd	30,2	21,6	14	15,9	8	19	19,7	11,7	3,7	3,5
Tb	5,8	4,3	2,7	3,1	1,9	3,5	3,7	1,6	0,5	0,9
Dy	37,4	28,1	17,6	19,7	12,2	22,9	23	7,6	2,6	6,2
Ho	7,4	5,7	3,5	4	2,5	4,5	4,5	1,2	0,4	1,3
Er	21,7	16,6	10,6	11,7	8	13,4	13	3	1,2	3,6
Tm	3,55	2,79	1,81	1,85	1,48	2,11	2,02	0,4	0,21	0,61

Yb	23,6	18,2	12,3	12,1	10,2	14,6	12,9	2,7	1,5	4,1
Lu	3,31	2,74	1,8	1,78	1,57	2,24	1,96	0,45	0,25	0,54

*Concentrations above the detection limit. Values are calculated based on the modal mineralogy, mineral chemistry and geochemistry.

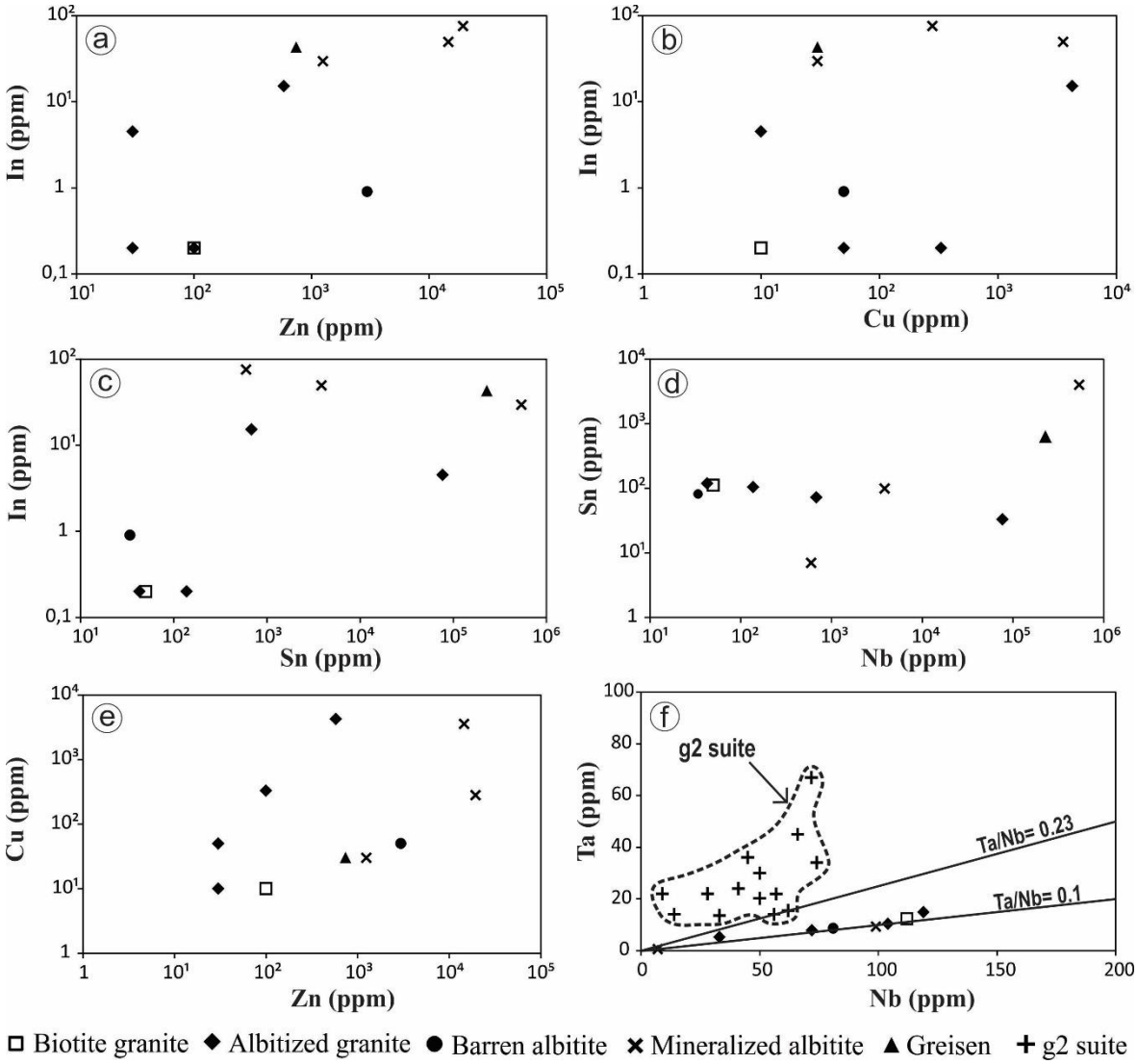

Figure 3. Binary plots of In vs Zn (a), In vs Cu (b), Sn vs In (c), Sn vs Nb (d) and Cu vs Zn (e) and Ta vs Nb (f) for samples from the biotite granite and mineralized zones of the Sucuri Massif. The circle in (f) highlights analyses from g2 suite. Note: g2 suite data from Botelho (1992), Moura (1993) and Moura et al., (2014).

4.3 In-bearing minerals

Indium concentration in the Earth's crust is relatively low (approximately 0.05 ppm for continental and 0.072 ppm for oceanic crust; Taylor & McLennan 1985), and the occurrence of indium minerals is very rare. Indium is a chalcophile element and is found in trace amounts in base metal sulfide minerals of zinc, copper, iron and tin. Among indium-bearing minerals, the highest concentrations occur in sphalerite, stannite, cassiterite and chalcopyrite (Schawarz-

Schampera & Herzing 2000). In the Sucuri Massif, the identified indium-bearing minerals are cassiterite, chalcopyrite and sphalerite. Although cassiterite is the most abundant ore mineral, higher concentrations of indium are normally associated with sphalerite crystals. Table 3 summarizes the concentrations of indium in sphalerite, chalcopyrite and cassiterite.

Table 3. Summary of Indium concentrations in sphalerite, cassiterite and chalcopyrite crystals from the Sucuri Massif. (n = number of analyses).

Mineral	n	Indium [wt.%]	
		range	average
sphalerite	79	0.05 - 0.45	0.235
cassiterite	93	0.08 - 0.211	0.145
chalcopyrite	35	0.04 - 0.145	0.079

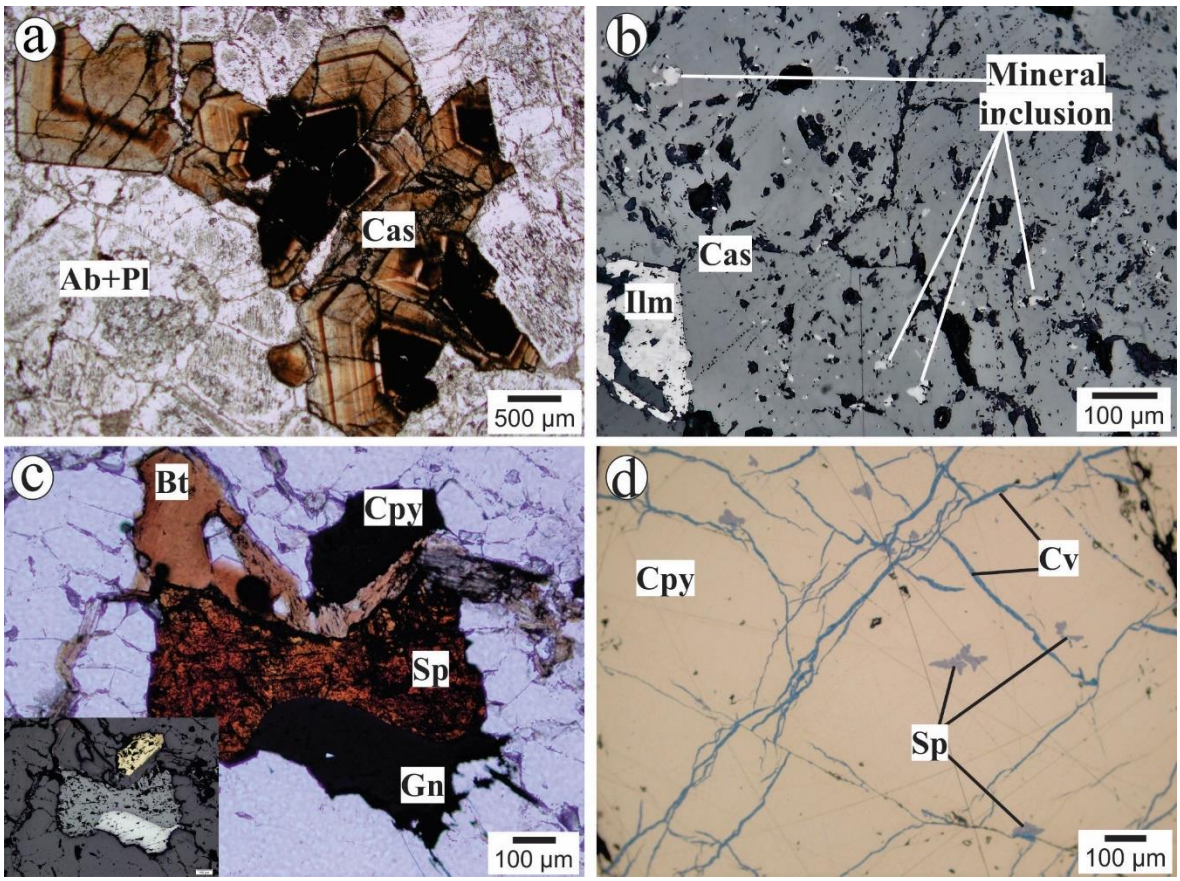

Figure 4. Photomicrographs of general textures of indium-bearing minerals from Sucuri massif. (a) Parallel and oscillatory zoning in cassiterite crystals, with the core darkish than border. (b) Inclusions of columbite-tantalite in cassiterite crystals. (c) Anhedral sphalerite crystal in equilibrium with galena, chalcopyrite and biotite; below, in the left corner, detail in reflected light, highlighting the sulfides. (d) Chalcopyrite crystal with irregular fractures filled by

covellite and hosting small sphalerite inclusions. Covellite is alteration product of chalcopyrite. Abbreviations Ab: albite; Bt: biotite; Cas: cassiterite; Cpy: chalcopyrite; Cv: covellite; Gn: ganela; Ilm: ilmenite; Pl: plagioclase; Sp: sphalerite.

4.3.1 Cassiterite

Cassiterite is the only tin-ore mineral and commonly occurs as agglomerates or as disseminated crystals up to 3 mm in size. It is associated with albite, quartz, sphalerite, chalcopyrite, ilmenite, and biotite and fluorite and beryllium minerals. In most cases, cassiterite has well-developed parallel and oscillatory zoning of varied thickness (Fig. 4a). However, less frequently, homogeneous crystals are also observed. The zonation is characterized by the alternation of bands with lighter color (colorless to light brown) and bands with darker color. Crystal cores are typically darker in comparison to outer borders. In addition, mineral inclusions up to 40 µm of columbo-tantalite, ilmenorutile, wolframite and ilmenite are observed (Fig. 4b).

To investigate the indium content and the trace elements (*i.e.*, Fe, Mn, Nb, Ta, Ti and W) that commonly replace Sn in the cassiterite lattice, a total of 93 EMPA analyses were carried out. In addition, the compositional variations of cassiterite may give clues about the involved genetic processes as well as the substitution mechanisms related to ore-forming environments (Steveson & Taylor 1973, Möller *et al.* 1988, Murciego *et al.* 1997). The results reveal that the concentrations of Nb_2O_5 (*i.e.*, up to 2 wt.%) are higher than those of Ta_2O_5 (*i.e.*, up to 0.1 wt.%), and the concentrations of Fe_2O_3 (*i.e.*, up to 0.7 wt.%) are higher than those of MnO (*i.e.*, up to 0.06 wt.%). Also significant are the TiO_2 concentrations of up to 1.34 wt.% and WO_3 concentrations of approximately 0.5 wt.%. Indium concentrations range from 800 to 2100 ppm. In general, the highest averages of indium contents are found in cassiterite from greisen (*i.e.*, 1522 ppm of In_2O_3), followed by albitized granite (*i.e.*, 1458 ppm of In_2O_3) and finally albitite (*i.e.*, 1300 ppm of In_2O_3).

Additionally, compositional traverses were performed to investigate the chemical shifts related to crystal zoning. Some studies show that chemical zoning can be related to Fe, Nb, Ta, W or U content (Izoret *et al.* 1985, Ogunbajo 1993, Neiva 1996, 2008, Chicharro *et al.* 2016). In this case, compositional traverses (Fig. 5) show that the Fe concentration changes according to the zoning pattern, whereas Nb, W, Ti and In have no correlation with the zonation pattern. Lighter zones are characterized by lower Fe concentrations, whereas the darker zones have higher Fe concentrations (Table 4, Fe-poor analyses 1 to 4 and Fe-rich analyses 5 to 7). In the

intermediary zones, iron concentrations are constrained between 0.2 to 0.4 wt.% Fe_2O_3 (Table 4, analyses 8-13).

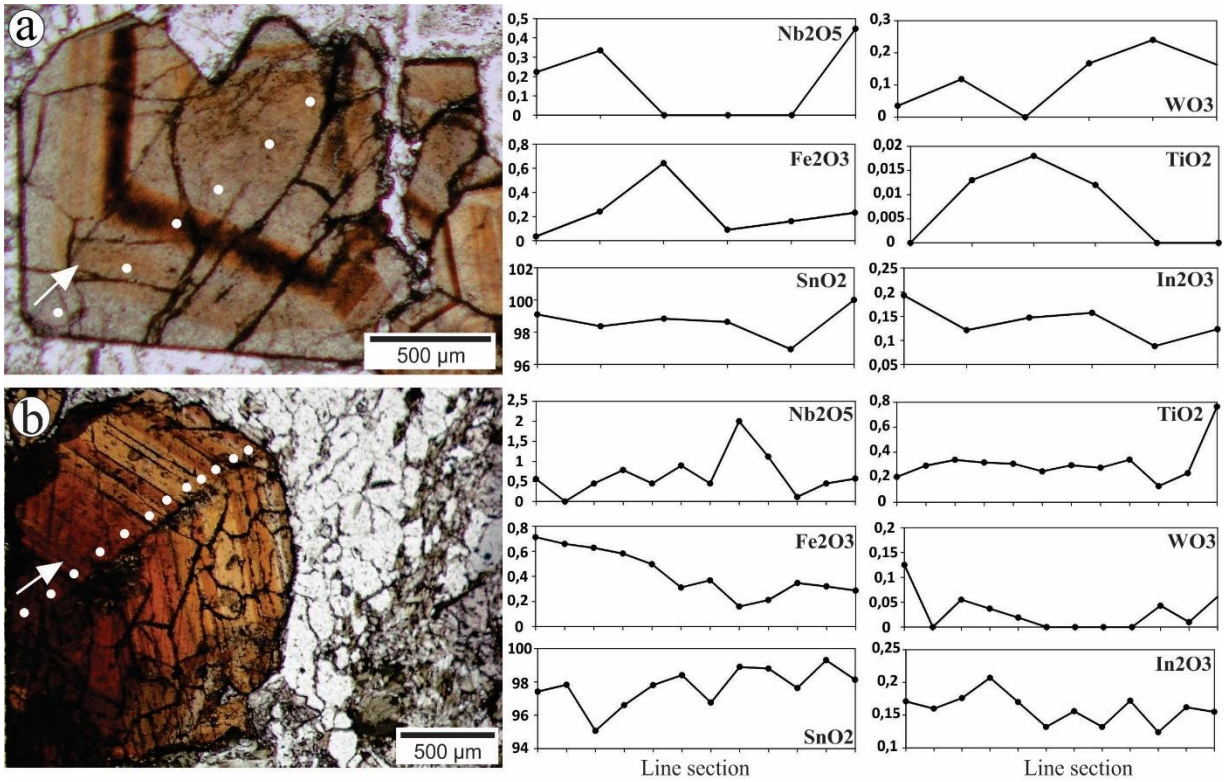

Figure 5. Traverse sections in zoned cassiterite crystals. The white points indicate the position of each analysis. The values of analysis are represented in percentage in weight. (a) Zoned cassiterite crystal from albitite with predominance of lighter zones. Note that there is no substitution correlation between the three represented elements. (b) Zoned cassiterite from greisen with a darker core in comparison to outside rims. Note the slightly increase in SnO_2 concentrations accompanied by the decrease in Fe_2O_3 concentrations.

The compositional variations of cassiterite between tin and trace elements are illustrated in Fig. 6. Tin shows a negative correlation with Fe, Nb, Ti and W. Moreover, only Nb has a correlation coefficient (R^2) near 0.99 (R^2 = 0.85) with Sn, suggesting substitution between the two elements. Iron, Ti and W have similar trends, increasing with decreasing Sn but with different degrees of correlation. Unlike other elements, indium shows independent correlation with Sn. Despite the large scattering of results, among all analyzed elements, Fe is the only element that shows a slightly positive correlation with In (Fig. 6).

Table 4. Representative cassiterite compositions from the Sucuri Massif. Cassiterite formulae was calculated on a basis of six oxygen atoms.

	Light zone				Dark zone			Intermediary zone					
	Greisen	Albitite	Albitized Granite	Albitite	Albitite	Albitized Granite	Greisen	Albitite	Greisen	Greisen	Albitite	Greisen	Albitite
	1	2	3	4	5	6	7	8	9	10	11	12	13
SnO2	98,04	99,76	99,80	99,36	98,73	98,01	98,11	99,04	98,68	96,95	97,21	98,77	98,14
Nb2O5	1,34	0,00	0,00	0,45	0,00	1,01	0,45	0,00	0,56	2,01	1,34	0,11	1,23
TiO2	0,08	0,00	0,08	0,00	0,29	0,00	0,01	0,03	0,26	0,41	1,34	0,00	0,08
In2O3	0,14	0,12	0,11	0,14	0,16	0,12	0,20	0,18	0,12	0,19	0,11	0,16	0,21
Fe2O3	0,00	0,09	0,00	0,02	0,66	0,67	0,70	0,11	0,26	0,32	0,34	0,36	0,42
ZnO	0,00	0,02	0,06	0,00	0,05	0,01	0,00	0,00	0,00	0,07	0,00	0,05	0,04
MnO	0,03	0,03	0,01	0,00	0,00	0,00	0,00	0,00	0,04	0,01	0,00	0,00	0,02
WO3	0,00	0,02	0,00	0,02	0,00	0,00	0,10	0,01	0,00	0,00	0,08	0,37	0,07
Ta2O5	0,00	0,00	0,00	0,00	0,00	0,00	0,00	0,14	0,00	0,00	0,06	0,00	0,00
UO2	0,00	0,00	0,00	0,09	0,01	0,03	0,00	0,00	0,01	0,00	0,02	0,00	0,00
PbO	0,00	0,02	0,00	0,00	0,02	0,02	0,00	0,00	0,00	0,00	0,00	0,04	0,01
Total	99,62	100,05	100,06	100,08	99,92	99,86	99,58	99,50	99,93	99,97	100,49	99,86	100,21
Sn	2,94	2,99	2,99	2,97	2,97	2,93	2,95	2,99	2,96	2,90	2,93	2,97	2,93
Nb	0,05	0,00	0,00	0,02	0,00	0,03	0,02	0,00	0,02	0,07	0,05	0,00	0,04
Ti	0,00	0,00	0,00	0,00	0,02	0,00	0,00	0,00	0,01	0,02	0,08	0,00	0,00
In	0,00	0,00	0,00	0,00	0,01	0,00	0,01	0,01	0,00	0,01	0,00	0,01	0,01
Fe	0,00	0,01	0,00	0,00	0,04	0,04	0,04	0,01	0,02	0,02	0,02	0,02	0,03
Zn	0,00	0,00	0,00	0,00	0,00	0,00	0,00	0,00	0,00	0,00	0,00	0,00	0,00
Mn	0,00	0,00	0,00	0,00	0,00	0,00	0,00	0,00	0,00	0,00	0,00	0,00	0,00
W	0,00	0,00	0,00	0,00	0,00	0,00	0,00	0,00	0,00	0,00	0,00	0,01	0,00
Ta	0,00	0,00	0,00	0,00	0,00	0,00	0,00	0,00	0,00	0,00	0,00	0,00	0,00
U	0,00	0,00	0,00	0,00	0,00	0,00	0,00	0,00	0,00	0,00	0,00	0,00	0,00
Pb	0,00	0,00	0,00	0,00	0,00	0,00	0,00	0,00	0,00	0,00	0,00	0,00	0,00
Total	3,00	3,01	3,01	3,00	3,04	3,01	3,02	3,01	3,02	3,02	3,07	3,01	3,01

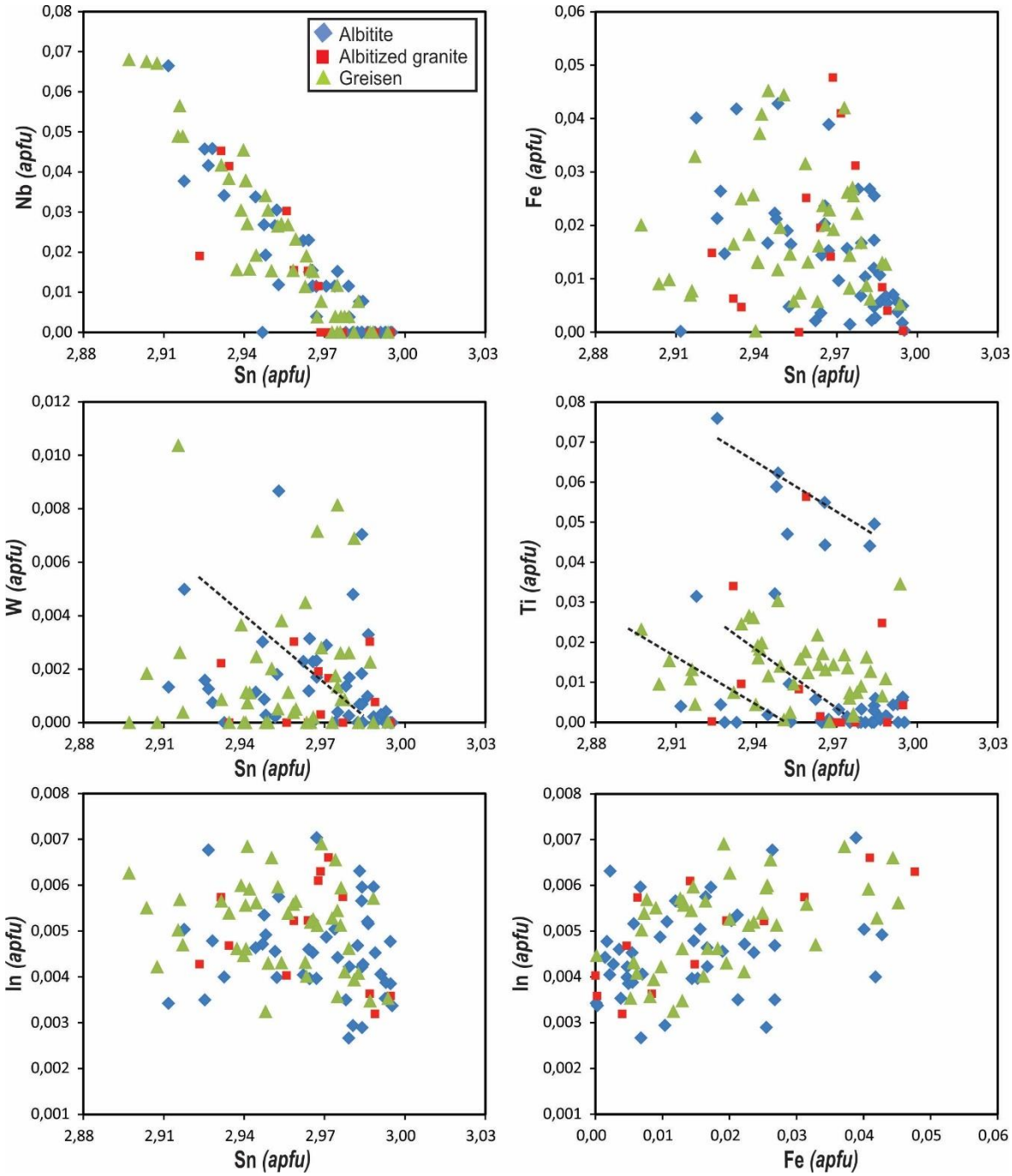

Figure 6. Binary diagrams showing the compositional variations of cassiterite according to Sn concentrations. The values are reported in number of atoms per formula unit (apfu). Good negative correlation occurs between Sn and Nb and independent correlation between Sn and In concentrations. Dashed lines show replacement trends.

Figure 7 illustrates cassiterite compositional variations in a ternary diagram. The heterogeneous distribution of minor and trace element results in different atomic ratios of (Fe,Mn)/(Nb,Ta) and suggests that Sn is replaced by different mechanisms. The following substitution equations have been proposed by different authors in studies of variations in

cassiterite compositions within Sn deposits worldwide (Moore & Howie 1979, Dulski *et al.* 1982, Wang 1988, Möller *et al.* 1988, Murciego 1990, Neiva 1996, Murciego *et al.* 1997, Cèrny *et al.* 2004, Lerouge *et al.* 2017).

The high values of Nb (i.e., 2 wt.% Nb_2O_5) in some analyses may be explained either by i. $(Nb,Ta)^{4+} \leftrightarrow Sn^{4+}$ or ii. $4(Nb,Ta)^{5+} \leftrightarrow 5Sn^{4+}$ (Möller et al., 1988). The replacement of Sn by Ta and Nb shown in i. is very limited because the existence of $(Ta,Nb)^{4+}$ requires unexpectedly low oxygen fugacity. Therefore, the second substitution is more likely to play a role in Fe-poor cassiterites. Only few analyses plot along the columbite-tantalite/ixiolite tie lines (Fig. 5b), suggesting that the substitution defined as $2(Nb,Ta)^{5+} + (Fe,Mn)^{2+} \leftrightarrow 3(Sn,Ti)^{4+}$ is not significant. For analyses with a (Fe,Mn)/(Ta,Nb) ratio between 0.5 and 1.0, which plot on the ixiolite and columbite tie lines, the substitution $(Ta,Nb)^{5+} + Fe^{3+} \leftrightarrow 2Sn^{4+}$ plays an important role in the incorporation of Nb and Fe in cassiterite. Analyses plotting close to or along the (SnTi) – (FeMn) edge might attest to the participation of the $Fe^{3+} + OH^{-} \leftrightarrow Sn^{4+} + O^{2-}$ substitution (Möller *et al.* 1988).

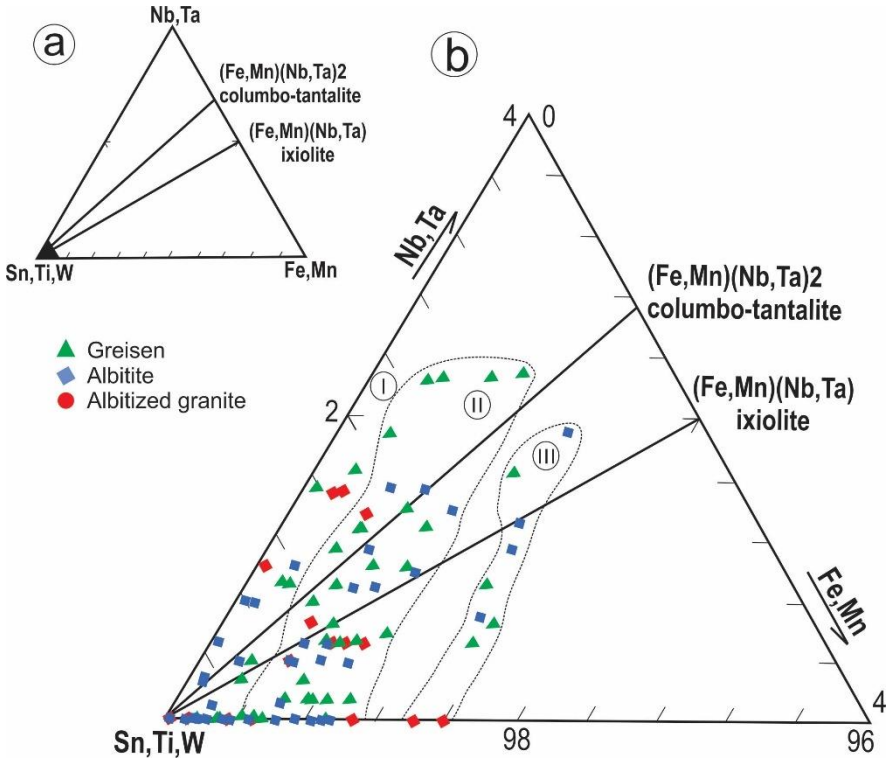

Figure 7. Compositional diagram of (Nb,Ta)–(Fe,Mn)–(Sn,Ti,W) showing cassiterite analyses from the Sucuri Massif. Diagram (a) shows the entire triangular plot, and (b) shows an

expansion of the (Sn,Ti) corner, from 100 to 96. The fields I, II and III represent the limit of lighter, intermediary and darker compositional zones of cassiterite crystals, respectively.

Another important feature is the correlation between Fe and W in some samples. Figure 8 is a binary plot illustrating the relation of the two elements. Analyses with a W/Fe atomic ratio of 1 indicate the presence of wolframite group minerals as solid solution (ferberite). Moreover, analyses with W/Fe atomic ratios of 0.5 indicate the presence of Fe_2WO_6 in solid solution (Serranti *et al.* 2002). Most analyses from the Sucuri Massif plot along or below the line with W/Fe atomic ratios of 0.5, suggesting that the substitution $W^{6+} + 2Fe^{3+} \leftrightarrow 3Sn^{4+}$ probably plays an important role during W incorporation in cassiterite (Möller *et al.* 1988). Cassiterite crystals with Nb, Ti and W contents higher than 1 wt.% were inspected in backscattered electron images. However, no inclusion and/or exsolution of other minerals was observed, supporting the hypothesis that Nb, Ti and W are confined to the cassiterite structure.

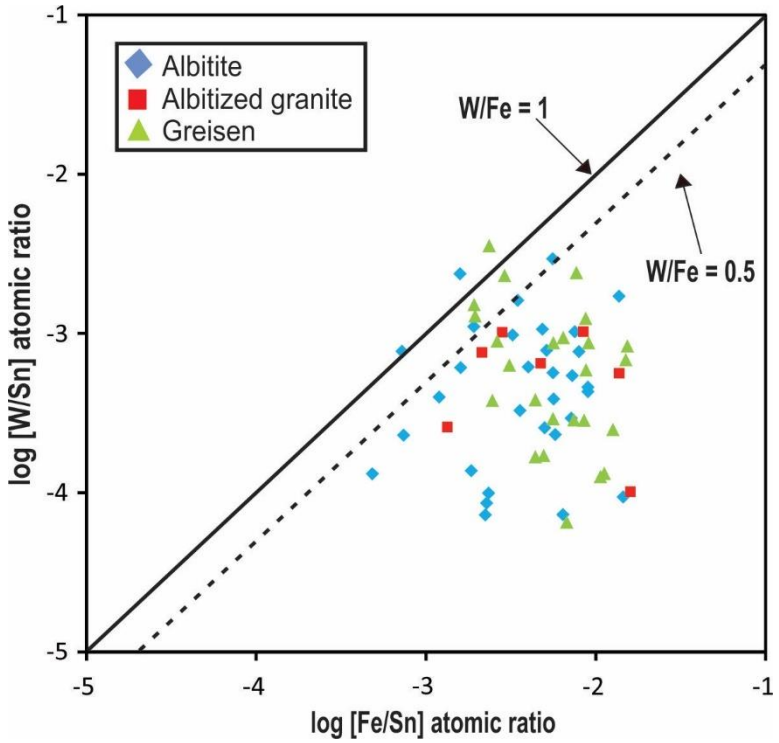

Figure 8. Plot of W/Sn vs Fe/Sn atomic ratios of cassiterite from different mineralized zones of the Sucuri Massif. The W/Fe ratios = 1 indicates the presence of wolframite inclusions whereas ratios below 0.5 indicate the presence of Fe_2WO_6 in the cassiterite structure. Note that most analyses has W/Fe atomic ratios bellow 0,5, thus supporting the presence of Fe_2WO_6 in the cassiterite structure (Serranti et al., 2002).

4.3.2 Sulfides

Sphalerite and chalcopyrite are the only In carriers among the sulfides identified in the Sucuri Massif. Sphalerite is homogeneous with reddish color and is commonly disseminated as anhedral grains up to 1.5 mm and associated with cassiterite, chalcopyrite, pyrite and galena. In addition, small inclusions are observed in chalcopyrite nodules (Fig. 4c and 4d). Chalcopyrite is a minor accessory mineral in the studied mineralized rocks. It occurs as irregular masses of several centimeters in size (*i.e.,* up to 4 cm) and as minor lamellae-shaped inclusions in sphalerite grains. The occurrence of chalcopyrite is more limited than those of cassiterite and sphalerite and is observed only in the albitized granite. Locally, larger masses of chalcopyrite contain sphalerite and pyrite inclusions and fractures filled by covellite (Fig. 4d).

Table 5. Representative compositions and structural formula of sphalerite and chalcopyrite from the Sucuri Massif.

Mineral	Sphalerite In-poor		Sphalerite In-rich			Chalcopyrite	
S (wt.%)	33,46	33,09	32,63	32,45	33,56	34,37	34,48
Zn	58,75	59,64	61,29	58,52	59,63	0,07	0,07
Fe	7,23	7,28	5,84	8,68	6,79	30,99	30,82
Cu	0,01	0,00	0,07	0,19	0,29	35,04	34,44
Cd	0,30	0,39	0,14	0,20	0,21	0,00	0,01
In	0,00	0,05	0,13	0,29	0,45	0,01	0,13
Sn	0,00	0,00	0,01	0,02	0,00	0,06	0,00
Ag	0,00	0,00	0,01	0,03	0,01	0,02	0,00
Pb	0,01	0,05	0,00	0,00	0,23	0,00	0,09
Sb	0,02	0,00	0,01	0,01	0,01	0,01	0,01
total	99,78	100,51	100,13	100,39	101,20	100,56	100,05
S (*apfu*)	1,01	0,99	0,99	0,98	1,00	1,96	1,98
Zn	0,87	0,88	0,91	0,86	0,87	0,00	0,00
Fe	0,12	0,13	0,10	0,15	0,12	1,02	1,02
Cu	0,00	0,00	0,00	0,00	0,00	1,02	1,00
Cd	0,00	0,00	0,00	0,00	0,00	0,00	0,00
In	0,00	0,00	0,00	0,00	0,00	0,00	0,00
Sn	0,00	0,00	0,00	0,00	0,00	0,00	0,00
Ag	0,00	0,00	0,00	0,00	0,00	0,00	0,00
Pb	0,00	0,00	0,00	0,00	0,00	0,00	0,00
Sb	0,00	0,00	0,00	0,00	0,00	0,00	0,00

A total of 79 and 35 EMPA analyses were carried out on sphalerite and chalcopyrite crystals, respectively. Table 5 summarizes the representative compositions of both minerals. Based on EMPA analyses, sphalerite crystals may be divided into In-poor (*i.e.*, less than 0.1 wt.% In) and In-rich (*i.e.,* from 0.1 to 0.45 wt.% In; Table 5). Indium-poor sphalerites occur in late quartz veins and barren albitite, while In-rich sphalerites are observed in tin-mineralized

zones. Indium-poor sphalerite also shows low Cu concentrations (*i.e.*, less than 0.1 wt.% Cu), high Cd concentrations (*i.e.*, up to 0.4 wt.% Cd) and approximately 7 wt.% Fe. Indium-rich sphalerites have slightly higher contents of Cu (*i.e.*, from 0.1 to 0.3 wt.%) and lower Cd contents (*i.e.*, less than 0.3 wt.%) compared to In-poor crystals. The highest Fe concentrations (*i.e.*, up to 8.7 wt.%; Table 4) occur in In-rich sphalerites, which have In concentrations of approximately 0.3 wt.%.

Figure 9 illustrates the concentrations of trace and major elements in sphalerite. Both In-rich and In-poor sphalerites show positive correlations between Cu and In concentrations (Fig. 9a) with In/Cu ratios near 1 (R^2 = 0.83). This association may suggest a substitution between these elements and Zn ($In^{3+} + Cu^{+} \leftrightarrow 2Zn^{2+}$), which is facilitated by the structural similarity between roquesite ($CuInS_2$) and sphalerite (Oen *et al.* 1980; Johan 1988). However, our results do not necessarily support this substitution as the process of incorporation of In in sphalerite, due to independent correlation between Cu+In and Zn. A negative correlation exists between In+Cu and Cd (Fig. 9b) and between Fe and Zn (Fig. 9c), reflecting the structural substitutions among these metals. In addition, the positive correlation observed between In+Cu and Fe (Fig. 9d) may contribute to the incorporation of indium in sphalerite.

The In concentrations in chalcopyrite are lower than those observed in other In-bearing minerals (*i.e.*, sphalerite and cassiterite), ranging from 0.01 to 0.13 wt.% (800 ppm on average). In many other regions of the world with In occurrences, chalcopyrite has normally low to moderate In contents, *i.e.*, Mount Pleasant (0.1 to 0.4 wt% In, Sinclar *et al.* 2006), Goka (0.34 to 0.48 wt.% In, Murao & Furuno 1990), Bingham District (3 to 1000 ppm In, Rose 1967), Baal Gammon (0.22 wt.% In, Andersen *et al.* 2016) and Mangabeira (0.2% In, Moura *et al.* 2007). Minor concentrations of zinc (i.e., up to 0.189 wt.%), lead (up to 0.237 wt.%), silver (up to 0.084 wt.%), cadmium (up to 0.068 wt.%) and tin (up to 0.1 wt.%) are also found in the chalcopyrite from the Sucuri Massif.

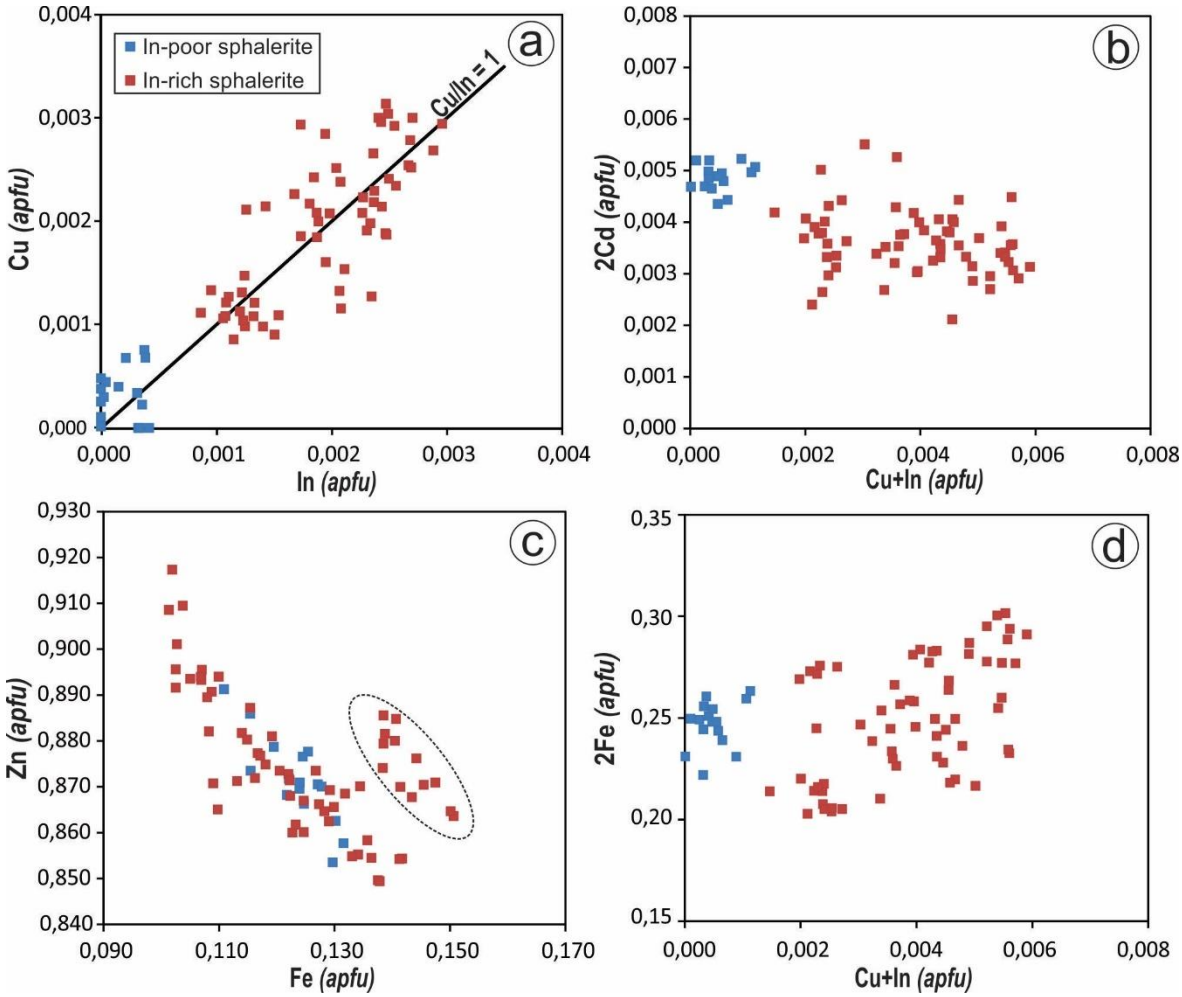

Figure 9. Binary diagram of Cu vs In (a), 2Cd vs Cu+In (b), Zn vs Fe (c) and 2Fe vs Cu+In (d) in sphalerite. The values are reported in number of atoms per formula unit (apfu). The circle in (c) highlights sphalerite analyses with approximately 8 wt.% of Fe.

5. Beryllium minerals

Beryllium minerals are best known from geologic systems associated with felsic magmatism, where they can have a magmatic or post-magmatic origin (Barton & Young 2002). The occurrence of beryllium minerals in hydrothermally altered rocks may provide some information about the chemical conditions of derived hydrothermal fluids, such as fluid alkalinity, sulfur and oxygen fugacities and aluminum and silica activities (Bilal & Fonteilles 1988, Barton & Young 2002).

In the Sucuri Massif, beryllium minerals were described for the first time by Bilal & Fonteilles (1988) and Bilal (1991). They include beryl ($Be_3Al_2Si_6O_{18}$), phenakite (Be_2SiO_4) and helvine group minerals (*i.e.*, $(Fe,Zn,Mn)_8Be_6(SiO_4)_6S_2$). Helvine group minerals form a solid

solution among three end members: helvine (Mn dominant), danalite (Fe dominant) and genthelvite (Zn dominant), and its structural formula is analogous to that of sodalite (*i.e.*, $Na_8Al_6(SiO_4)_6Cl_2$; Hassan & Grundy 1984, 1985).

Beryl and phenakite are present only in the greisen, associated with quartz, muscovite and cassiterite (Fig. 10a). Beryl is euhedral to round shaped, up to 5 cm, greenish colored and locally altered to fine-grained muscovite. Phenakite is thinner (*i.e.*, up to 2 mm) and commonly rounded and locally occurs associated with garnet (Fig. 10b). Helvine is commonly euhedral (*i.e.*, up to 2 mm) and colorless to slightly brown, occurring in all hydrothermalized zones. Particularly in the greisen, helvine occurs as irregular grains replacing garnet and phenakite (Fig. 10b).

Representative EMPA values for the helvine group are listed in Table 6. The ternary diagram for helvine group minerals (Fig. 11) illustrates compositional variations among the end members (*i.e.*, genthelvite, helvine and danalite). Based on mineral associations and EMPA analyses, helvine is divided in four groups according to the host rock. Helvine from barren albitite shows chemical zonation, with the cores dominated by genthelvite ($He_{28}Da_8Ge_{64}$) and the rims dominated by danalite ($He_{26}Da_{44}Ge_{30}$). This zoned helvine typically occurs associated with albite, fluorite, chalcopyrite, sphalerite and biotite. Helvine from albitized granite shows no major compositional variation, typically having 54% danalite, 22% helvine and 24% genthelvite (Fig. 11). It occurs normally associated with quartz, albite/microcline, fluorite, biotite, chalcopyrite and sphalerite (Fig. 10c). Within the greisen, helvine has two distinct compositions due to the occurrence of garnet. Helvine that grows from garnet grains (*i.e.*, 77% spessartine and 22% almandine) is enriched in Mn and depleted in Zn ($He_{60-42}Da_{39-53}Ge_{1-5}$; Fig. 11), whereas in garnet-free greisen, helvine has little compositional variation ($He_{23-26}Da_{41-54}Ge_{36-20}$; Fig. 11).

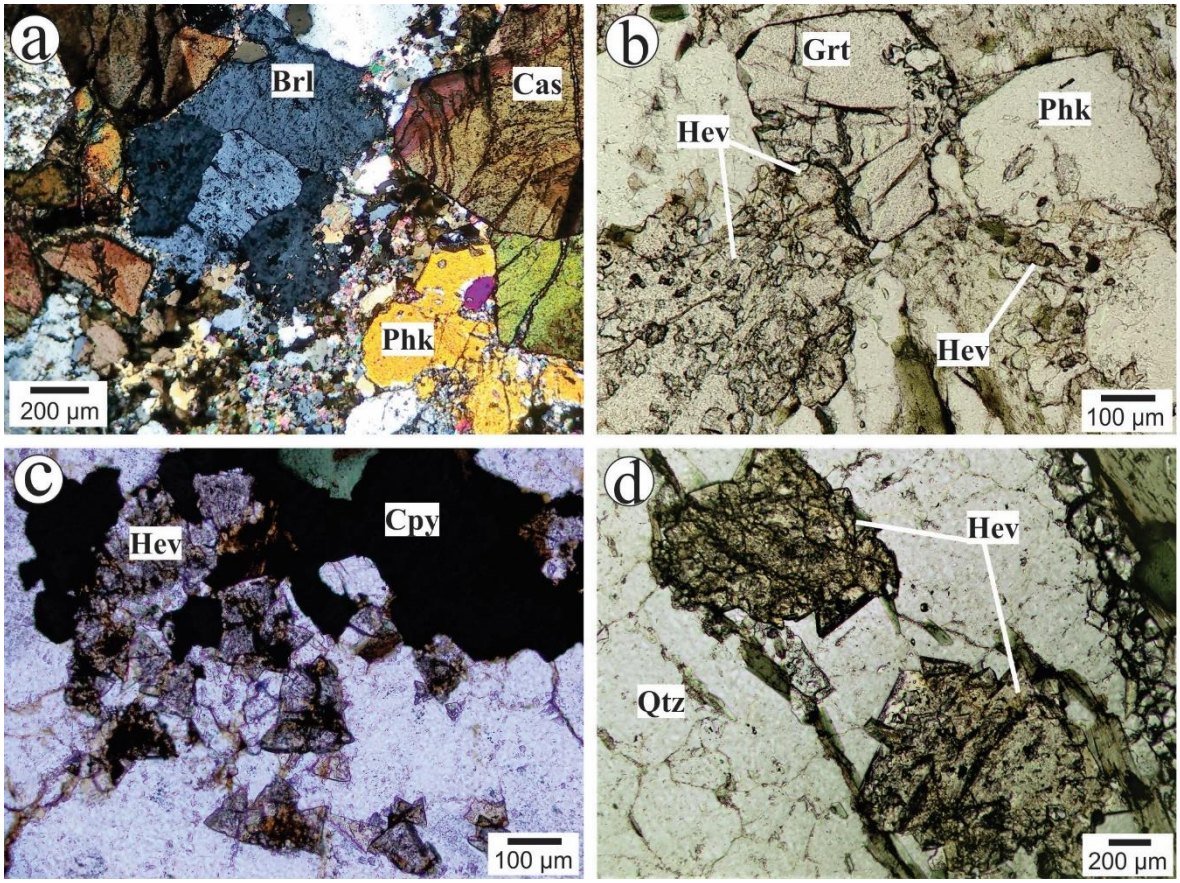

Figure 10. Photomicrographs of beryllium minerals showing the relationship with other minerals. (a) Beryl and phenakite crystals from greisen, in equilibrium with cassiterite and quartz (crossed polarizers). (b) Garnet and phenakite crystals in disequilibrium contact with helvine (He_{60-42}-Da_{39-53}-Ge_{1-5}). Sample from garnet-bearing greisen. (c) Small helvine crystals (He_{22}-Da_{54}-Ge_{24}) associated with chalcopyrite and biotite. Sample from albitized granite. (d) Helvine light brown coloration from cassiterite-quartz vein (He_{31-55}-Da_{54-31}-Ge_{15-14}). Abbreviations Brl: beryl; Cas: cassiterite; Grt: garnet; Hev: helvite; Phk: phenakite; Qtz: quartz and Cpy: chalcopyrite.

The last group is represented by helvine crystals that occur in small quartz-biotite-rich veinlets. This group is dominated by brownish crystals (Fig. 10d), which show a wide variation between danalite and helvine compositions, with approximately 15% genthelvite ($He_{31-55}Da_{54-31}Ge_{15-14}$; Fig. 11). However, helvine from this group shows extensive variations in Mn and Fe concentrations, and garnet is not observed.

Table 6. Representative helvine group minerals compositions from the Sucuri Massif.

Sample	Barren albitite	Barren albitite	Albitized granite	Albitized granite	Garnet greisen	Garnet greisen	Garnet-free greisen	Garnet-free greisen	Biotite quartz vein	Biotite quartz vein
wt.%										
SiO2	34,87	33,89	34,92	32,29	33,45	33,18	34,60	35,48	32,02	34,11
BeO	12,25	12,95	12,75	13,10	13,30	13,23	12,37	12,63	13,15	12,92
Al2O3	0,00	0,04	0,03	0,05	0,01	0,02	0,05	0,01	0,07	0,05
FeO	3,96	21,91	26,06	27,26	19,76	27,23	19,39	23,62	26,88	13,15
MnO	12,91	12,67	10,63	10,20	30,66	20,94	10,77	11,46	15,53	23,31
ZnO	33,88	16,84	13,63	14,30	0,17	2,58	19,38	14,91	8,83	14,46
MgO	0,00	0,00	0,00	0,00	0,01	0,00	0,00	0,00	0,00	0,00
CaO	0,06	0,00	0,04	0,02	0,04	0,02	0,04	0,00	0,03	0,00
Na2O	0,00	0,00	0,00	0,00	0,01	0,00	0,00	0,00	0,00	0,00
K2O	0,03	0,00	0,02	0,00	0,04	0,02	0,05	0,01	0,04	0,01
TiO2	0,12	0,14	0,00	0,23	0,00	0,03	0,00	0,00	0,00	0,00
S	5,35	5,56	5,76	5,39	5,52	5,35	5,70	5,86	5,29	5,24
O=S	-2,68	-2,78	-2,88	-2,69	-2,76	-2,68	-2,85	-2,93	-2,64	-2,62
Total	100,75	101,21	100,95	100,13	100,20	99,92	99,50	101,06	99,20	100,64
Structural formula based 13 O										
Si	3,27	3,13	3,21	3,03	3,07	3,07	3,24	3,25	3,02	3,15
Be	2,76	2,88	2,82	2,96	2,94	2,94	2,79	2,78	2,98	2,87
Al	0,00	0,00	0,00	0,00	0,00	0,00	0,00	0,00	0,01	0,00
Total	6,03	6,01	6,03	5,99	6,01	6,01	6,03	6,04	6,00	6,02
Fe	0,31	1,69	2,00	2,14	1,52	2,10	1,52	1,81	2,12	1,02
Mn	1,03	0,99	0,83	0,81	2,38	1,64	0,86	0,89	1,24	1,82
Zn	2,34	1,15	0,93	0,99	0,01	0,18	1,34	1,01	0,61	0,99
Mg	0,00	0,00	0,00	0,00	0,00	0,00	0,00	0,00	0,00	0,00
Ca	0,01	0,00	0,00	0,00	0,00	0,00	0,00	0,00	0,00	0,00
Na	0,00	0,00	0,00	0,00	0,00	0,00	0,00	0,00	0,00	0,00
K	0,00	0,00	0,00	0,00	0,00	0,00	0,01	0,00	0,00	0,00
Ti	0,01	0,01	0,00	0,02	0,00	0,00	0,00	0,00	0,00	0,00
S	0,94	0,97	0,99	0,95	0,95	0,93	1,00	1,01	0,94	0,91
Total	10,67	10,82	10,78	10,90	10,88	10,86	10,76	10,76	10,92	10,76
Mol% of poles										
HE(Mn)	27,86	25,87	22,04	20,57	60,92	41,81	23,01	23,99	31,21	47,67
GE(Zn)	63,71	29,97	24,64	25,15	0,30	4,49	36,09	27,20	15,47	25,78
DA(Fe)	8,43	44,16	53,33	54,29	38,78	53,70	40,90	48,81	53,32	26,55

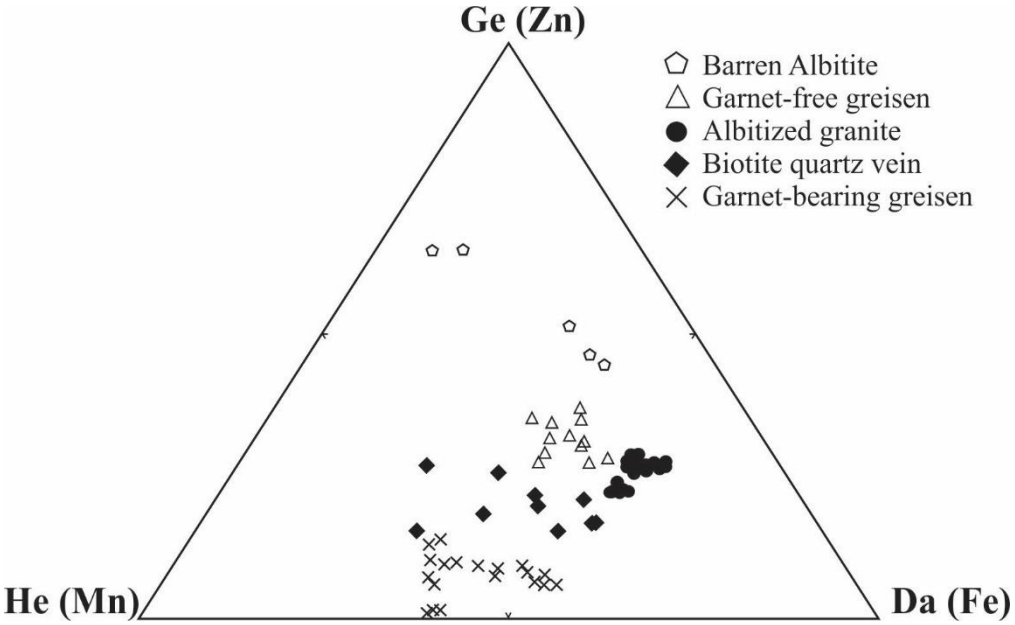

Figure 11. Ternary diagram for classification of helvine group minerals, based on helvine (He), genthelvite (Ge) and danalite (Da). The helvine group minerals have been divided into five groups, according to their hosting rock.

5.1 Helvine Stability

The composition of helvine group minerals is directly affected by the presence of phenakite + sulfide + silicate (Barton & Young, 2002). Therefore, the restricted occurrence of helvine group minerals results from the restricted stability field of the cited minerals. These minerals are sensitive to the redox and sulfidation states, as well as to the alkalinity of the system. Favorable conditions for the formation of helvine group minerals are constrained to the stability conditions for coexisting sulfides and silicates (Burt 1980, 1988; Fig. 12). Danalite occurs in reduced and low sulfidation state environments, whereas genthelvite is stable in more alkaline conditions. Helvine is normally observed in more sulfidized and Mn-rich systems, crystallizing at moderate oxygen fugacities and broader sulfur fugacities compared to genthelvite. The equations that describe the stability fields of these minerals are reported by Burt (1980, 1988) and Bilal & Fonteilles (1988, 1991).

The large compositional variations observed in helvine group minerals from the studied samples suggest different conditions of formation. The majority of helvine crystals from the Sucuri massif are rich in the danalite molecule (*i.e.*, approximately 50%). According to Burt (1980), the formation of danalite is given by the equation: $8Fe + 3SiO_2 + 3Be_2SiO_4 + 3O_2 + S_2 \leftrightarrow Fe_8Be_6Si_6O_{24}S_2$. Such a process requires an output of Fe in the system and a limited interval

of oxygen and sulfur fugacities as illustrated in Fig. 10. The occurrence of zoned crystals (*i.e.*, cores dominated by genthelvite and rims by danalite) suggests a change in the physicochemical conditions during crystallization. The albitization process increases the alkalinity of the system and may thus favor the formation of genthelvite. During crystallization, with an increase in sulfur fugacity, Zn tends to link with sulfur because Zn has a greater affinity for sulfur than Fe does, and danalite crystallization is favored via $Zn_8Be_6Si_6O_{24}S_2 + 8FeS_2 \leftrightarrow Fe_8Be_6Si_6O_{24}S_2 + 8ZnS + 4S_2$ (Bilal 1994). In the garnet greisen, the formation of Mn-rich helvine crystals may be explained by their coexistence with garnet. According to Bilal (1994), the formation of helvine from garnet and phenakite may occur during albitization processes and is represented as $8Mn_3Al_2Si_3O_{12} + 9Be_2SiO_4 + 8Na_2O + 33SiO_2 + 3S_2 \leftrightarrow 3Mn_8Be_6Si_6O_{24}S_2 + 16NaAlSi_3O_8 + 3O_2$. On the other hand, the helvine from cassiterite quartz veins is enriched in Mn, which is not attributed to association with garnet.

The elements that compose helvine group minerals (*i.e.*, Be, Zn, Mn, and S) are commonly found as trace elements in highly fractionated granitic systems. Therefore, the presence of helvine group minerals is typical of highly fractionated and alkaline granitic systems and indicates significant changes in sulfur and oxygen fugacities during their crystallization (Burt 1977, Bilal & Fonteilles 1988, Bilal 1991, Zito & Hanson 2017). The results from the present study disagree in part with the conclusions of Bilal (1994), showing that crystals with compositions closest to the helvine end member (*i.e.*, 61% of the Mn-rich member; Fig. 11) are restricted to the presence of garnet. Additionally, the absence of genthelvite in other hydrothermalized zones is attributed to the fact that these zones probably did not achieve the required alkalinity conditions. In summary, the predominance of danalite over helvine and genthelvite suggests limited conditions for oxygen and sulfur fugacities (*i.e.*, favoring danalite stability; Fig. 12), minor alkalinity, and an external input of Fe into the hydrothermal system.

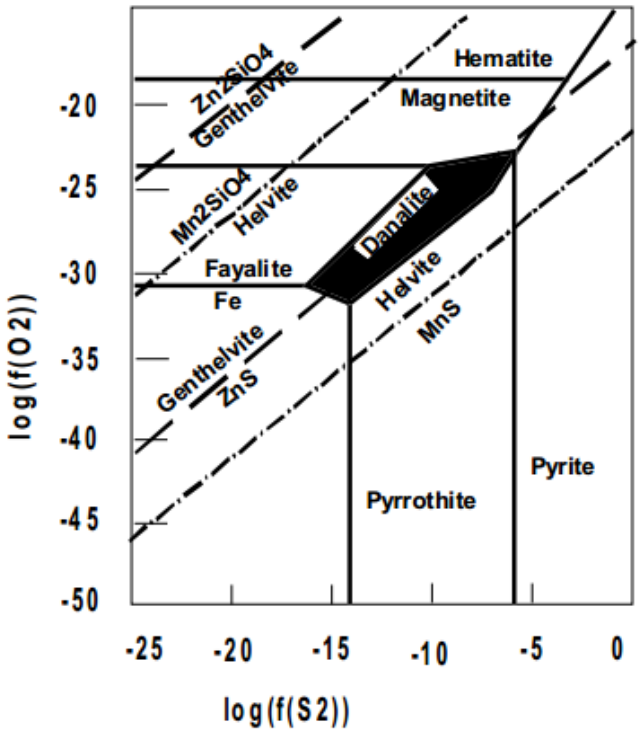

Figure 12. Stability fields of helvine group minerals in the f(O_2) versus f(S_2) diagram. The dark field represents the restrict domain the oxygen and sulfur fugacities where danalite is stable. Thermodynamic data after Robie et al. (1979) and Fursenko (1989).

6. Fluid inclusion

Fluid inclusion studies were performed on non-altered beryl- and cassiterite-bearing samples from mineralized greisen and albitite, respectively. Cassiterite crystals from the greisen are mostly dark brown; thus, fluid inclusion studies on this mineral are restricted to crystals from the albitite, which are lighter. The investigation aims to describe primary fluid inclusions in order to characterize hydrothermal fluids from distinct mineralized zones. Based on petrographic observations, fluid inclusions are divided into single- and two-phase inclusions (*i.e.*, only liquid and liquid + vapor bubble). Single-phase fluid inclusions are less abundant and occur only within beryl crystals. They are characterized by irregular shapes and composed of only a liquid phase. Due to their small size (*i.e.*, <5 μm), microthermometric measures were not performed in these inclusions.

Beryl hosts two distinct styles of primary fluid inclusions with two phases: i. tubular inclusions aligned parallel to the c-axis of the crystals (*i.e.*, usually up to 40 μm long; Fig. 13a) and ii. irregular to round shaped inclusions (*i.e.*, usually up to 20 μm in diameter; Fig. 13b).

Following Shepherd *et al.* (1985), the degree of fill (F) at room temperature for inclusion types i. and ii. varies from 0.7 to 0.95.

Cassiterite crystals host only one type of fluid inclusions, which are elongated to round shaped and normally uncolored. These inclusions are randomly distributed and do not seem to have any spatial relation to crystal zonation. In comparison to the fluid inclusions observed in beryl, the inclusions in cassiterite are generally smaller (typically 10 μm but reaching up to 20 μm; Fig. 13c and 13d). At room temperature, the F varies from 0.8 to 0.95, with rare exceptions of approximately 0.7. Inclusions smaller than 5 μm were not submitted to microthermometric measurements due to the difficulty of seeing the vapor bubble. Apart from fluid inclusions, ilmenite and niobium minerals are present as microinclusions (up to 10 μm: Fig. 13d) within cassiterite crystals.

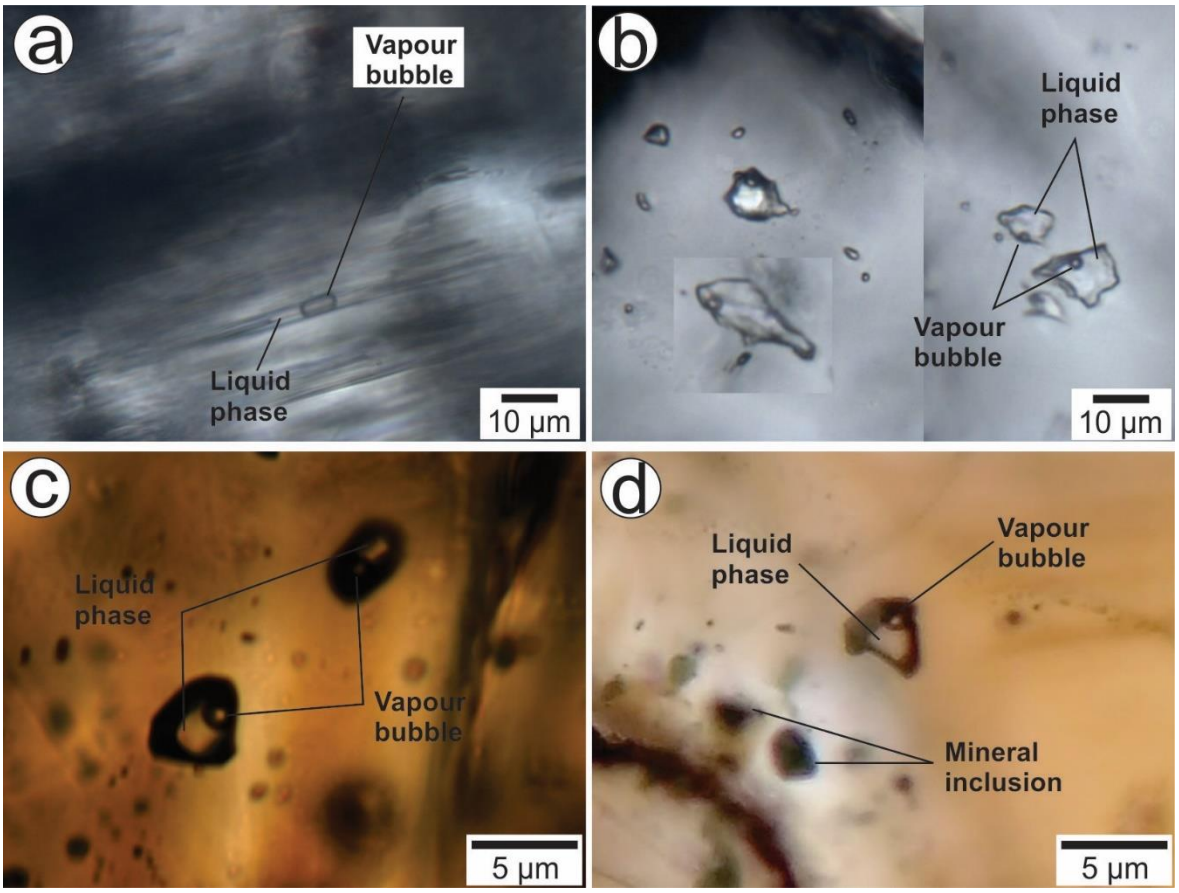

Figura 13. Photomicrographs show different fluid inclusion from the Sucuri massif. (a) Fluid inclusion aligned within c-axis of beryl crystal (type i. in the text). (b) Fluid inclusions randomly distributed within beryl crystal (type ii. in the text). (c) Fluid inclusions with two phases (liquid and vapor) enclosed within cassiterite crystal. (d) Fluid inclusions with two phases (liquid and vapor) enclosed within cassiterite crystal. Note the presence of micro inclusions of ilmenite crystals next to the fluid inclusion.

6.1 Microthermometry

During microthermometric measurements, eutectic (Te), final ice melting (Tm_{ice}) and homogenization (Th) temperatures were determined. Salinity values were calculated using the equation proposed by Bodnar (1993) for salinities lower than 23.2 wt.% NaCl equivalent. The obtained results are summarized in Table 7 and described as follows.

Table 7. Summary of main characteristics of fluid inclusions from the Sucuri Massif. L= liquid, V = vapor and F = degree of fill (Shepherd et al., 1985).

Host Mineral	Beryl	Cassiterite
Occurence	Tubular cavities, parallel to c-axis and irregular to round.	Elongate to round and uncolored
Size (μm)	6 - 40	5 - 10
Composition	H2O-NaCl	H2O-NaCl
Degree of fill (F)	0.7 - 0.95	0.8 - 0.95
Microthermometry		
Te (°C)	-39.9 to -18.3	-38.9 to -28.1
Tm_{ice} (°C)	-7.9 to -0.9	-6.8 to -0.8
Th (°C)	106 to 196	160 to 200
Salinity (wt.% NaCl)	0 - 11.6	1.4 - 10.2

Both types of fluid inclusions from beryl completely freeze at approximately -50ºC. Eutectic temperatures vary from -40 to -18ºC with modal values constrained between -24 and -20ºC (n = 38; Fig. 14a). These inclusions have ice melting temperature ranging from -8 to 0ºC (n = 67; Fig. 14b), which correspond to salinities varying from 0 to 11.6 wt.% NaCl equivalent. Heating tests show that fluid inclusions typically homogenize to a liquid phase. The total homogenization temperatures range from 106 to 196ºC (n = 53) with a higher frequency at approximately 120°C (Fig. 14c).

Accurate microthermometric analyses, mainly eutectic temperatures, of cassiterite-hosted fluid inclusions are limited by the sizes of the inclusions and the high birefringence of the hosting mineral. In the freezing tests, fluid inclusions completely freeze at approximately -65 º C. Only five successful measurements of eutectic temperatures were obtained, with values ranging between -38.1 to -29.1ºC. Ice melting temperatures (n = 55) vary from -6.8 to -0.8ºC, with modal values of approximately -3ºC (Fig. 13b), which correspond to salinities varying

from 1.4 to 10.2 wt.% NaCl equivalent. All fluid inclusions also homogenize to a liquid phase, with total homogenization temperatures varying from 160 to 200ºC (n = 42) and a higher frequency at approximately 180 ºC (Fig. 14c).

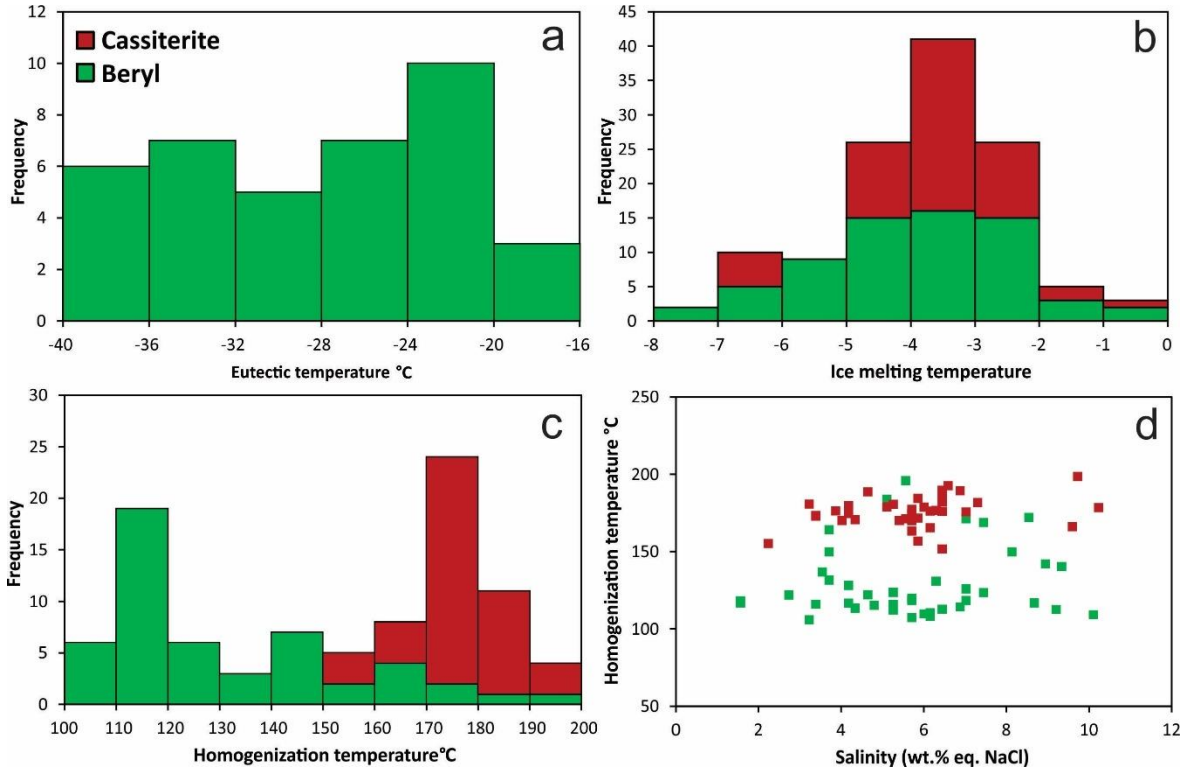

Figura 14. Histograms of obtained results from studied fluid inclusions of beryl and cassiterite crystals from the Sucuri massif. a) Beryl eutectic temperatures. b) Ice melting temperatures. c) Total homogenization temperatures. d) Plot of total homogenization temperatures versus salinities from aqueous inclusions of beryl and cassiterite crystals. Note that fluid inclusions hosted in cassiterite crystals have higher homogenization temperatures.

6.2 Implications

The reported petrographic and microthermometric data support that fluid inclusions hosted by cassiterite and beryl are similar. The studied aqueous fluid inclusions consist basically of two phases (*i.e.*, liquid and vapor) and have low salinity and homogenization temperatures. In diverse microthermometric studies of fluid systems, eutectic temperatures are used to qualitatively constrain the bulk chemistry of the system (Davis *et al.* 1990). The eutectic temperatures of the beryl-hosted fluid inclusions show wide variations (*i.e.*, most frequent intervals from -36 to -32ºC and from -28 to -20ºC). These results suggest that the fluid system is not only composed of Na but also contains K, Fe, Mn, Sn, In and Zn. The presence of these

metals in the system is also compatible with the presence of helvine group minerals and sulfides in the mineral assemblages.

Salinities and homogenization temperature do not seem to have any correlations in our results (Fig. 14d). Therefore, the only difference between fluid inclusions from beryl and those from cassiterite are the homogenization temperatures. Fluid inclusions in cassiterite have higher homogenization temperatures than those in beryl (Fig. 14d), indicating that cassiterite has a minimum crystallization temperature higher than that of beryl.

7. Sulfur isotopes

Galena, pyrite, sphalerite and chalcopyrite from mineralized zones were analyzed, and the sulfur isotope data are summarized in Table 7. All the $\delta^{34}S_{CDT}$ values from different samples are slightly negative and lie within the same variation range (*i.e.*, ranging from -4.86 to -1.52‰). Following the geothermometry criteria of mineral pairs (Ohmoto & Rye 1979), one mineral pair was used to estimate the deposition temperature. The co-genetic pair analyzed was sphalerite-chalcopyrite from albitized granite. Following Ohmoto & Rye (1979) and Campbell & Larson (1998), the estimated deposition temperature is approximately 230°C (Table 8). This temperature is compatible with the highest temperatures obtained from the fluid inclusion analyses (Table 8).

Table 8. Sulfur isotope data from mineralized zones of the Sucuri Massif. Values are reported in per mil values ($\delta^{34}S$‰) referenced to the CDT (Canyon Diable Troilite) standard.

Sample	Mineral	$\delta^{34}S_{CDT}$ (‰)	Temperature (°C)*
Albitized granite	Galena	-4,86	
Albitized granite	Pyrite	-2,64	
Quartz vein	Sphalerite	-1,52	
Albitized granite	Chalcopyrite	-3,39	230.2
Albitized granite	Sphalerite	-3,98	

*Isotopic temperature obtained for the sphalerite-chalcopyrite pair following Ohmoto and Rye (1979), and Campbell and Larson (1998).

8. Discussions and Conclusions

Several tin mineralizations in the Goiás Tin Province are assumed to have a hydrothermal origin, related to a F-enrichment in the hydrothermal fluids that favors the

transport of Sn and In (Botelho& Moura 1998, Moura *et al.* 2014). The Sucuri Massif is not different, as the hydrothermal zones are fluorine-rich. Based on geochemical data, the In content is controlled mainly by the contents of Zn and Cu, whereas Nb is related to Sn. In addition, Ta/Nb ratios are also important indicators of genetic processes of the mineralization in the region. According to Botelho & Moura (1998), apart from petrological characteristics, the g1 and g2 suites can be distinguished by their Ta/Nb ratios (Fig. 3f). The natural enrichment of Nb over Ta in the mineralized zones suggests that tin mineralization in the Sucuri Massif is associated with the g1 suite.

The main In-bearing minerals observed in the tin ore from the Sucuri Massif are cassiterite, sphalerite and chalcopyrite. Microprobe analyses reveal important concentrations of Ti, Fe, Nb, Mn, Ta and W in cassiterite. The incorporation of these metals in cassiterite is due to their similarity to Sn (*i.e.*, ionic radius and charge). The studied cassiterite crystals display remarkable chemical zoning, with the alternation of darker (Fe-rich) and lighter (Fe-poor) bands (Fig. 5). This zonation supports oscillatory variations in the composition of the mineralizing fluids. That the Fe, Nb, Ti and W concentrations are higher than those of Ta and Mn yields clues about the natural abundance of these elements in the system. Mossbauer and EPR studies in tin deposits (Möller *et al.* 1988, Murciego *et al.* 1997) reveal that in cassiterite crystals crystallized at high temperatures (*i.e.*, over 300ºC), the composition is dominated by Fe^{2+}. However, cassiterite crystals that crystallized at medium to low temperatures (*i.e.*, below 300ºC) incorporate mainly Fe^{3+}. Therefore, the homogenization temperatures of approximately 180 ºC are also in agreement with the predominance of Fe in the trivalent state. Moreover, the presence of Fe^{3+} may also explain the lack of correlation between Fe/Mn and Nb/Ta (Fig. 5), in response to the substitution $2(Nb,Ta)^{5+} + (Fe,Mn)^{2+} \leftrightarrow 3(Sn,Ti)^{4+}$. This inference supports the conclusion that the main mechanisms of substitution that occurred in the studied samples are i. $4(Nb,Ta)^{5+} \leftrightarrow 5Sn^{4+}$, ii. $(Nb,Ta)^{5+} + Fe^{3+} \leftrightarrow 2Sn^{4+}$ and iii. $Fe^{3+} + OH^{-} \leftrightarrow Sn^{4+} + O^{2-}$ (Moller *et al.* 1988).

The incorporation of indium and the formation of indium-bearing sulfides may result from i. the coupled substitution of iron, copper, tin and arsenic, ii. the incorporation into the tetrahedrally coordinated lattice positions and iii. the formation of submicroscopic inclusions of indium minerals (Schwarz-Schampera 2014). Sphalerite is the most important indium-bearing mineral. The coupled occurrence of In and Cu in sphalerite, according to previously published studies, suggests that the incorporation of In into sphalerite is substantially enhanced

if the Cu activity is elevated in the mineralizing hydrothermal fluid. Several studies have shown that In incorporation in sphalerite is via the coupled substitution $2Zn^{2+} \leftrightarrow Cu^{+} + In^{3+}$ (Johan 1988, Pattrick *et al.* 1993, Schorr & Wagner 2005, Cook *et al.* 2009, 2012). However, the obtained results do not support this proposition and suggest that Fe plays an important role in the incorporation of indium. Thus, in our samples, the incorporation of In into sphalerite is probably given by $3Zn^{2+} \leftrightarrow Cu^{+} + In^{3+} + Fe^{2+}$. Additionally, although the exact substitution that allows the incorporation of In into the chalcopyrite structure is still debated, some hypotheses have been proposed (Huston *et al.* 1995, Cook *et al.* 2011c). The most supported substitution is between Fe and In, probably in a solid solution between chalcopyrite and roquesite ($Cu^{+}Fe^{3+}S_2 \leftrightarrow Cu^{+}In^{3+}S_2$), given their similar structures. Finally, the incorporation of In into cassiterite is poorly constrained. However, in an effort to understand the process of indium incorporation and assuming that In is present as In^{3+} in the crust (Smith *et al.* 1978), recent studies propose that In correlates with Fe^{3+} for substitution with Sn (Lerouge *et al.* 2017). Considering that In and Fe are positively correlated in microprobe analyses ($R^2 = 0.2$; Fig. 4) and that most Fe is present as Fe^{3+}, the incorporation of In in cassiterite may be controlled by the following equations: i. $(Ta,Nb)^{5+} + (Fe,In)^{3+} \leftrightarrow 2Sn^{4+}$; ii. $W^{6+} + 2(Fe,In)^{3+} \leftrightarrow 3Sn^{4+}$ and iii. $(Fe,In)^{3+} + OH^{-} \leftrightarrow Sn^{4+}$.

The fluid inclusions in cassiterite and beryl support that the idea that fluids from the mineralizing system are purely aqueous (*i.e.,* without CO_2). Additionally, wide variations in the eutectic temperatures indicate that the fluids carried a diverse association of metals (Na^{+}, K^{+}, Fe^{3+}, Mn^{2+}). The low ice-melting temperatures and consequently low salinities of the inclusions (up to 11 wt.% NaCl eq.) are compatible with other studies of granite-related tin mineralization in hydrothermal systems (Lehmann 1990). These results are normally attributed to the mixture of magmatic (*i.e.,* high-salinity) and meteoric (*i.e.,* low-salinity) fluids, which triggers the ore precipitation (Wilkinson 2001). The temperature at which cassiterite forms in tin deposits is commonly from 300-500°C, as first shown by Little (1960) and later confirmed by various investigations (*e.g.,* Giuliani 1984, Giuliani *et al.* 1988, Wilkinson 1990). However, the homogenization temperatures for fluid inclusions in cassiterite from the Sucuri ore are approximately 180°C, which is below the expected value. However, values below 300°C have also been reported (Mount Pleasant: from 146 to 162°C, Elmi Assadzadeh *et al.* 2017). Furthermore, the temperature obtained from the co-genetic pair sphalerite-chalcopyrite

(~230°C) is compatible with the fluid inclusion results, suggesting that the system formed under lower temperature conditions.

In addition to fluid inclusion data, the helvine group minerals provide some insights about the mineralizing fluid. The predominance of danalite over helvine and genthelvite suggests a large availability of Fe in the system and very limited ranges for fS_2 and fO_2, conditions that coincide with the pyrrhotite domain (Fig. 12). Further, the Zn- and Mn-rich end members are formed in totally distinct hydrothermal zones. The Zn-rich end member occurs in albitites, while the Mn-rich end member is associated with quartz veins.

Sulfur isotopes are commonly used to constrain the source of S in different systems (Seal *et al.* 2006). Sulfur minerals from magmatic sources have $\delta^{34}S$ values constrained between -5 and 5‰ (Ohmoto & Rye, 1979). The obtained values of $\delta^{34}S$ (*i.e.*, -4.86 to -1.52‰) are compatible with a magmatic signature. Therefore, the granitic magma represents a possible source for the sulfur in the hydrothermal system. Several granite-related In-bearing deposits worldwide also show $\delta^{34}S$ values compatible with a magmatic sulfur source (Fig. 15).

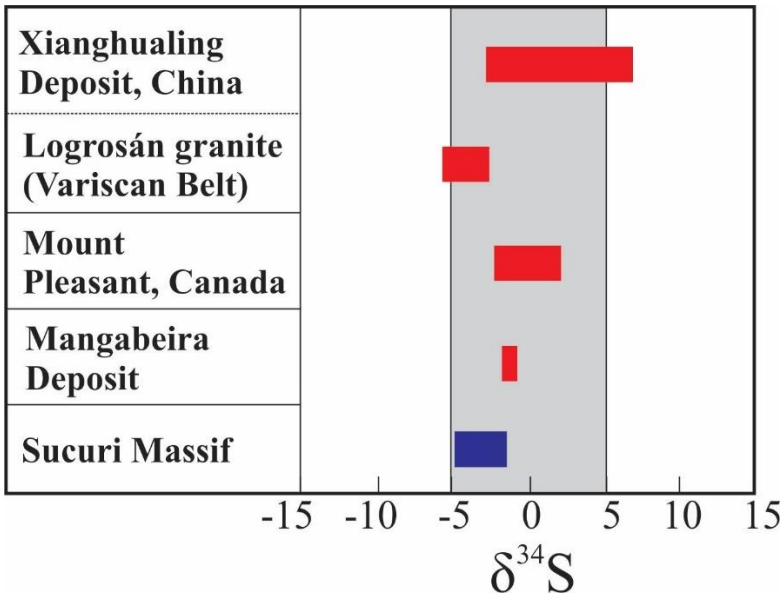

Figure 15. Relation of the $\delta^{34}S$ data for In-bearing tin deposits worldwide. The field in grey indicates sulfur from magmatic sources interval. References – Mangabeira, Moura et al., 2014; Variscan belt, Chicharro et al., 2016; Mount Pleasant deposit; and Xianghualing deposit, Liu, et al, 2017.

The obtained results of this work and the data from the literature support the hypothesis of two episodes of mineralization in the Goiás Tin Province, both formed with magmatic contributions. The first episode is related to the emplacement of the g1 suite, which involves less-evolved granite and a low-salinity and low-temperature hydrothermal system. This system is responsible for the generation of minor In-bearing tin deposits, similar to the Sucuri area, hosted by albitites and greisen veins. The second episode is related to the emplacement of the g2 suite. This system involves a highly evolved granite, with major tin-indium deposits in greisenized cupolas generated by complex hydrothermal fluids (H_2O–NaCl–KCl–CO_2) with temperature above 300 ºC.

Acknowledgments

This study was supported by CNPq (Conselho Nacional de Desenvolvimento Científico e Teconológico) under grant 131743/2016-3 to ACRM and grant 311203/2014-0 to NFB. Analytical facilities of the Instituto de Geociências of the University of Brasília (UnB) provided additional support for this research. The authors thank laboratory technicians for technical support during thin section confection, and microprobe and sulfur isotopes analyzes.

9. References

Andersen, J.C.O., Stickland, R.J., Rollinson, G.K., Shail, R.K., 2016. Indium mineralisation in SW England: host parageneses and mineralogical relations. Ore Geology Reviews 78, 213-238.

Barton, M.D. and Young, S., 2002. Non-pegmatitic deposits of beryllium: mineralogy, geology, phase equilibria and origin, *in* Grew, E.S., ed., Beryllium: Mineralogy, petrology and geochemistry: Reviews in Mineralogy and Geochemistry 50, 591-691.

Bastos Neto, A.C., Ferron, J.T.M.M., Chauvet, A., Chemale, F., Lima, E.F., Barbanson, L., Costa, C.F.M., 2014. U-Pb dating of the Madeira Suite and structural control of the albite-enriched granite at Pitinga (Amazonia, Brazil): evolution of the A-type magmatism and implications for the genesis of the Madeira Sn-Ta-Nb (REE, cryolite) world-class deposit. Precambrian Research 243, 181-196.

Bettencourt, J.S., 1997. Tin-bearing granites from Brazil: a review. In: II International Symposium on Granites and Associated Mineralization, Salvador, Brazil, Extend Abstracts, pp. 34-35.

Bettencourt, J.S., Leite Jr., W.B., Goraieb, C.L., Sparremberg, I., Bello, R.M. S., Payolla, B.L., 2005. Sn-polymetallic greisen-type deposits associated with late-stage rapakivi granites, Brazil: fluid inclusions and stable-isotopes characteristics. Lithos 80, 363-386.

Bettencourt, J.S., Juliani, C., Xavier, R.P., Monteiro, L.V.S., Bastos Neto, A.C., Klein, E.L., Assis, R.R., Leite Junior., W.B., Moreto, C.P.N., Fernandes, C.M.D., Pereira, V.P., 2016. Metallogenetic systems associated with granitoid magmatism in the Amazonian Craton: An overview of the present level of understanding and exploration significance. Journal of South American Earth Sciences 68, 22-49.

Bilal, E., 1991. Etude de deux massifs de la province granitique stannifere de l' etat de Goias (Brésil) et des formations metasomatiques associees aux mineralisations en Sn et Be. Paris, 480p. (PhD Thesis. Ecole des Mines de Paris). (Unpublished).

Bilal, E., 1994. Geochimie et conditions de cristallisation des minéraux du groupe de l'helvite. Geonomos –V.2 n.2.

Bilal, E. and Fonteilles, M. 1988. Conditions d'apparition respectives de l'helvite, de la phénacite et du béryl dans l'environnement granitique: exemple du massif de Sucuri (Brésil). C.R. Acad. Sci. Paris, t. 307, série II: 273-276.

Bilal, E., Moutte, J., Botelho, N.F., Marini, O.J. and Andrade, G.F., 1997. Geochemistry of two Proterozoic A-type granites of Goias State, Brazil: possible links with rapakivi series. Anais da Academia Brasileira de Ciências 69(3), 349-365.

Bodnar, R.J., 1993. Revised equation and table for determining the freezing point depression of H2O–NaCl solutions. Geochimica Cosmochimica Acta 57, 683-684.

Borges, R.M.K., Villas, R.N.N., Fuzikawa, K., Dall'Agnol, R., Pimenta, M.A., 2009. Phase separation, fluid mixing, and origin of the greisens and potassic episyenite associated with the Água Boa pluton, Pitinga tin province, Amazonian Craton, Brazil. Journal of South American Earth Sciences 27, 161-183.

Botelho, N.F., 1992. Les ensembles granitiques subalcalins à peralumineux mineralisés em Sn et In de la Sous-Province Paranã, Etat de Goias, Brésil: Unpublished PhD Thesis, Univ. Paris VI, 343 pp.

Botelho, N.F. and Moura, M.A., 1998. Granite-ore deposit relationship in central Brazil. Journal of South American Earth Sciences 11, 427-438.

Botelho, N.F. & Roger, G., 1990. Découverte de minéraux d'indium dans la paragenèse sulfurée du gîte stannifère protérozoïque de Mangabeira, Goiás, Brésil. C.R. Acad. Sci. Paris 310, 247-253.

Botelho, N.F., Roger, G., d'Yvoire, F., Moëlo, Y. & Volfinger, M., 1994, Yanomamite, InAsO4•2H2O, a new indium mineral from topaz-bearing greisen in the Goiás Tin Province, Brazil. European Journal of Mineralogy 6, 245-254.

Burt, D.M., 1977. Chalcophile-lithophile tendencies in the helvite group: genthelvite stability in the system ZnO–BeO–Al2O3–SiO2–SO–1–F2O–1 (abstract). American Geophysical Union Transactions 58, 1242.

Burt, D.M. 1980. The stability of danalite $Fe_3Be_3(SiO_4)_3S$. American Mineralogist 65, 355-360.

Burt, D.M., 1988. Stability of genthelvite, $Zn_3Be_3(SiO_4)_3S$: an exercise in chalcophilicity using exchange operators. American Mineralogist 73, 1384-1394.

Campbell, A.R., and Larson, P.B., 1998, Introduction to stable isotope applications in hydrothermal systems, in Richards, J.P., and Larson, P.B., eds., Techniques in hydrothermal ore deposits geology: Reviews in Economic Geology 10, 173-193.

Černý, P., 1991. Fertile granites of Precambrian rare-element pegmatite fields: is geochemistry controlled by tectonic setting or source lithologies. Precambrian Research 51, 429-468.

Černý, P., Chapman, R., Ferreira, K., Smeds, S.-A., 2004. Geochemistry of oxide minerals of Nb, Ta, Sn and Sb in the Varuträsk granitic pegmatite, Sweden: The case of an "anomalous" columbite-tantalite trend. American Mineralogist 89, 505-518.

Chicharro, E., Boiron, M-C., López-Garcia, J.A., Barfod, D.N., Villaseca, C., 2016. Origin, ore forming fluid evolution and timing of the Logrosán Sn–(W) ore deposits (Central Iberian Zone, Spain). Ore Geology Reviews, 72, 896-913.

Cook, N.J., Ciobanu, C.L., Pring, A., Skinner, W., Shimizu, M., Danyushevsky, L., Saini-Eidukat, B., Melcher, F., 2009. Trace and minor elements in sphalerite: a LA-ICPMS study. Geochimica Cosmochimica Acta, 73, 4761-4791.

Cook NJ, Ciobanu CL, Brugger J, Etschmann B, Howard DL, de Jonge MD, Ryan C, Paterson D (2012) Determination of the oxidation state of Cu in substituted Cu-In-Fe-bearing sphalerite via μ-XANES spectroscopy. American Mineralogist 97(2-3), 476-479.

Cook, N.J., Sundblad, K.L., Valkama, M., Nygard, R., Ciobanu, C.L., 2011c. Indium mineralization in A-type granites in south-eastern Finland: insights into mineralogy and partitioning between coexisting minerals. Chemical Geology 284, 62-73.

Davis, D.W., Lowenstein, T.K., Spencer, R.J., 1990. Melting behavior of fluid inclusions in laboratory-grown halite crystals in the systems NaCl–H2O, NaCl–KCl–H2O, NaCl–MgCl2–H2O and NaCl– CaCl2–H2O. Geochimica Cosmochimica Acta 54, 591-601.

Dulski, P., Möller, P., Villalpando, A. and Schneider, H.J., 1982. Correlation of trace element fractionation in cassiterites with the genesis of the Bolivian Metallotect. In: Metallization Associated with Acid Magmatism (Ed. A.M. Evans), 71-83.

Dunn, P.J., 1976. Genthelvite and the helvine group. Mineralogical Magazine 40, 627-636.

Elmi Assadzadeh, G., Samson, I.M., Gangon, J.E., 2017. Evidence for aqueous liquid-liquid immiscibility in highly evolved tin-bearing granites, Mount Pleasant, New Brunswick, Canada. Chemical Geology 448, 123-136.

Fursenko, D.A., 1989. Uslovija sinteza mineralov gruppy gel'vina. Izd. Nauka, Sibirskoe Otdelenie, Novosibirsk, 76 p.

Genkin A.D., and Murav'eva, I.V., 1963. Indite and jalindite, new indium minerals. Zap. Vses. Mineralog. Obshchestva 62, 445.

Giuliani, G., 1984. Les concentrations filoniennes à tungstène-étain du massif granitique des Zaër (Maroc Central): minéralisations et phases fluides associées. Mineralium Deposita 19, 193-201.

Giuliani, G., Li, Y.D., Sheng, T.F., 1988. Fluid inclusion study of Xihuashan tungsten deposit in the southern Jiangxi province, China. Mineralium Deposita 23, 24-33.

Hassan, I. & Grundy, H.D. 1984. The crystal structures of sodalite-group of minerals. Acta Crystallographica B40, 6-13.

Hassan, I. & Grundy, H.D. 1985. The crystal structures of helvite group minerals, $(Mn,Fe,Zn)_8Be_6Si_6O_24S_2$. American Mineralogist, 70, 186-192.

Huston, D.L., Sie, S.H., Suter, G.F, Cooke, D.R., Both, R.A., 1995. Trace elements in sulfide minerals from eastern Australian volcanic-hosted massive sulfide deposits; Part I, Proton microprobe analyses of pyrite, chalcopyrite, and sphalerite, and Part II, Selenium levels in pyrite; comparison with delta 34 S values and implications for the source of sulfur in volcanogenic hydrothermal systems. Economic Geology 87, 785-811.

Ivanov V.V., 1963. Indium in some igneous rocks of the USSR. Geochem 12, pp. 115.

Izoret, L., Marnier, G., Dusausoy, Y., 1985. Caractérisation cristallochimique de la cassitérite des gisements d'etain et de tungtène de Galice, Espagne. Canadian Mineralogist 23, 221-231.

Johan, Z., 1988. Indium and germanium in the structure of sphalerite: an example of coupled substitution with copper. Mineralogy and Petrology 39, 211-229

Kato, A., 1965. Sakuraiite, a new mineral (in Japanese). Chigaku Kenkyu, Sakurai Volume: 1-5.

Kissin, S.A., and Owens, D.R., 1989. The relatives of stannite in the light of the new data. Canadian Mineralogist 27, 673-688.

Lehmann, B., 1990. Metallogeny of tin. Lecture notes in earth sciences 32. Springer-Verlag, 211 pp.

Lenharo, S.L.R., Moura, M.A., Botelho, N.F., 2002.Petrogenetic and mineralization processes in Paleo- to Mesoproterozoic rapakivi granites: example from Pitinga and Goiás, Brazil. Precambrian Research 119, 277-299.

Lerouge, C., Gloaguen, E., Wille, G., Bailly, L., 2017. Distribution of In and other rare metals in cassiterite and associated minerals in Sn ± W ore deposits of the western Variscan Belt. European Journal Mineralogy 29, 739-753.

Liu, J., Rong, Y., Zhang, Liu, Z., Chen, W., 2017. Indium Mineralization in the Xianghualing Sn-Polymetallic Orefield in Southern Hunan, Southern China. Minerals 7(9), 173.

Mandarino, J.A., 1996. New minerals recently approved by the Commission on New Minerals and Mineral Names International Mineralogical Association. European Journal Mineral 8, 1213-1222.

Marini, O.J. and Botelho, N.F., 1986, A província de granitos estaníferos de Goiás. Revista Brasileira de Geociências 16, 119-131.

Möller, P., Dulski, P., Szacki, W., Malow, G., Riedel, E., 1988. Substitution of tin in cassiterite by tantalum, niobium, tungsten, iron and manganese. Geochimica Cosmochimica Acta, 52, 1497-1503.

Moore, F. and Howie, R.A. 1979. Geochemistry of some Cornubian cassiterites. Mineralium Deposita 14(1), 103-107.

Moura, M.A., Botelho, N.F., Mendonça, F.C., 2007. The indium-rich sulfides and rare arsenates of the Sn–In mineralized Mangabeira A-type granite, Central Brazil. Canadian Mineralogist. 45, 485-496.

Moura, M.A., Botelho, N.F., Olivo, G.R., Kyser, Kurt, Pontes, R. M., 2014. Genesis of the Proterozoic Mangabeira tin–indium mineralization, Central Brazil: Evidence from geology, petrology, fluid inclusion and stable isotope data. Ore Geology Reviews. 60, 36-49.

Murao, S., and Furuno, M., 1990. Indium-bearing ore from the Goka Mine, Naegi District, Southwestern Japan. Mining Geology 40, 35-42.

Murciego, A. 1990. Estudio mineralógico y cristaloquímico de la casiterita. Relación con su genesis. PhD. Thesis, Univ. Salamanca. 610 pp.

Murciego, A., Garciasanchez, A., Dusausoy, Y., Martin Pozas, J.M. & Ruck, R., 1997. Geochemistry and EPR of cassiterites from the Iberian Hercynian Massif. Mineralogical Magazine 61, 357-365.

Neiva, A.M.R., 1996. Geochemistry of cassiterite and its inclusions and exsolution products from tin and tungsten deposits in Portugal. Canadian Mineralogist 34, 745-768.

Neiva, A.M.R., 2008. Geochemistry of cassiterite and wolframite from tin and tungsten quartz veins in Portugal. Ore Geology Reviews, 33, 221-238.

Oen, I.S., Kager, P., Kieft, C., 1980.Oscillatory zoning of a discontinuous soild-solution series: sphalerite-stannite. American Mineralogist 65, 1220-1232.

Ogunbajo, M.I., 1993. The mineralogy and geochemistry of some cassiterite from the Younger Granite province of the Jos plateau, Nigeria. Journal of African Earth Sciences 16(4), 465-472.

Ohmoto, H.Y., Rye, R.O., 1979. Isotopes of sulfur and carbon. En: Geochemistry of Hydrothermal Ore Deposits. J. Wiley and Sons, New York, pp. 509-567.

Pattrick R.A.D., Dorling M., Polya D.A., 1993. TEM study of indium- and copper-bearing growth-banded sphalerite. Canadian Mineralogist 31(1), 105-117

Pavlova, G.G., Palessky, S.V., Borisenko, A.S., Vladimirov, A.G., Seifert, T., Phan, A., 2015, Indium in cassiterite and ores of tin deposits. Ore Geology Reviews, 66, 99–13.

Picot, P., Pierrot, R., 1963. La roquésite, premier minerál d'indium, CuInS (sub 2). Bulletin de la Société Française de Minéralogie et de Cristallographie 86, 7 – 14.

Pimentel, M.M., Fuck, R.A., Botelho, N.F., 1999. Granites and the geodynamic evolution of the Neoproterozoic Brasilia Belt, Central Brazil. Lithos 46, 463–483.

Razin, L.V., Rudashevskii, N.S., Sidorenko, G.A., 1981. Tolovkite. Zap. Vses. Min. Obshchn 110: 474.

Robie, R.A., Hemingway, B.S., Fisher, J.R., 1979. Thermodynamic Properties of Minerals and Related Substances at 298.15 K and 1 Bar (105 Pascals) Pressure and at Higher Temperatures. Geological Survey Bull., nº 1452, 456 p.

Rose, A.W., 1967. Trace elements in sulfide minerals from Central district, New Mexico and Binghman district, Utah, Geochimica Cosmochimica Acta 31, 547-585.

Schwartz-Schampera, U., Herzig, P.M., 2002, Indium - Geology, Mineralogy and Economics. Springer-Verlag Berlin Heidelberg, New York (257 pp.).

Schwarz-Schampera U., 2014 Indium. In: Gunn G (ed) Critical metals handbook. Wiley, Hoboken, pp 204–229.

Schorr S., Wagner G., 2005. Structure and phase relations of the Zn2x(CuIn)1−xS2 solid solution series. J Alloys Compd 396 (1–2): 202–207.

Seal, R.R., 2006. Sulfur isotope geochemistry of sulfide minerals. Reviews in Mineralogy and Geochemistry 61, 633-677.

Seifert, T. 2008. Metallogeny and petrogenesis of lamprophyres in the mid-European variscides-post-collisional magmatism and its relationship to late-variscan ore forming processes (Bohemian Massif). IOS Press BV, Amsterdam, Netherlands, 303 p

Seifert, T., Chaplygin, I.V., Yudovskaya, M.A., Chaplygin, O. 2015. Mantle-derived In mineralization in the Erzgebirge and Kuril Island Arc.in "Goldschmidt Conference 2015, Prague, Czech Republic", Goldschmidt Abstracts, 2835

Serranti, S., Ferrini, V., Masi, U., Cabri, L.J., 2002. Trace-element distribution in cassiterite and sulfides from rubané and massive ores of the Corvo deposit, Portugal. Canadian Mineralogist 40, 815–835

Shepherd, T.J., Rankin, A.H., Alderton, D.H.M., 1985. A Practical Guide to Fluid Inclusion Studies. Blackie and Son, New York (239 pp.)

Sinclair, W.D., Kooiman, G.J.A., Martin, D.A., Kjarsgaard, I.M., 2006.Geology, geochemistry and mineralogy of indium resources at Mount Pleasant, New Brunswick, Canada. Ore Geology Reviews. 28, 123–145.

Smith, I.C., Carson, B.L., Hoffmeister, F., 1978. Trace metals in the environment, Volume 5 – Indium. Ann Arbor Science Publishers, 552 p.

Stevenson, B.G. and Taylor, R.G., 1973. Trace element contents of some cassiterites from Eastern Australia. Proc. R. Sac. Queensland, 84 (3), 43-54.

Taylor, S.R., and McLennan, S.M., 1985. The continental crust: its composition and evolution. Blackwell Science.

Valkama, M., Sundblad, K., Nygård, R., Cook, N., 2016. Mineralogy and geochemistry of indium-bearing polymetallic veins in the Sarvlaxviken area, Lovisa, Finland. Ore Geology Reviews, 75, 206–219.

Wang. R., 1988. Etude minéralogique et cristallochmique de cassitérite, niobotantalates et minéraux disséminés du granite de Beauvoir (Allier): Implications métallogéniques. Thése de 1'Université P. Sabatier, Toulouse. 204pp.

Werner, T.T., Mudd, G.M., Jowitt, S.M. (2017): The world's byproduct and critical metal resources part III: a global assessment of indium. Ore Geology Reviews, 86, 939–956

Wilkinson, J.J., 1990. The role of metamorphic fluids in the development of the Cornubian Orefield: fluid inclusion evidence from south Cornwall. Mineralogical Magazine 54, 219-230.

Wilkinson, J.J., 2001. Fluid inclusions in hydrothermal ore deposits. Lithos 55, 229-272.

Yu, T. H., Lin, S.L., Chao, P., Fang, C.S., Huang, C.S., 1974. Yixunite. Acta Geol. Sinica 2. 202 (abstract in American Mineralogist 61, p. 165).

Zito, G., and Hanson, S.L., 2017. Genthelvite overgrowths on danalite cores from a pegmatite miarolitic cavity in Cheyenne Canyon, El Paso County, Colorado. Canadian Mineralogist 55, 195-206

Capitulo 4 – Conclusão da Dissertação

Os dados obtidos neste trabalho permitem concluir que:

- Ao contrário do que ocorre nos outros depósitos da província, onde a mineralização é hospedada em cúpolas greisenizadas, no maciço Sucuri as principais zonas mineralizadas em estanho e índio são albititos e restritos greisens.
- Os principais minerais que contêm índio identificados no Maciço Sucuri são: cassiterita, esfalerita e calcopirita. A cassiterita é o minério mais abundante, porém as maiores concentrações de índio são encontradas na esfalerita (até 0,4% em peso de In).
- Os principais mecanismos de incorporação de índio na cassiterita são definidos por: i. $(Ta,Nb)^{5+} + (Fe,In)^{3+} \leftrightarrow 2Sn^{4+}$; ii. $W^{6+} + 2(Fe,In)^{3+} \leftrightarrow 3Sn^{4+}$ e iii. $(Fe,In)^{3+} + OH^{-} \leftrightarrow Sn^{4+}$. Já para a esfalerita, devido a forte relação entre índio, cobre e ferro a incorporação de índiofoi definida por: $3Zn^{2+} \leftrightarrow Cu^{+} + In^{3+} + Fe^{2+}$. Para a calcopirita propõe-se sua similaridade estrutural com a roquesita ($Cu^{+}Fe^{3+}S_2 \leftrightarrow Cu^{+}In^{3+}S_2$), onde há uma troca entre ferro e índio.
- O estudo de inclusões fluidas revelou fluidos puramente aquosos, com baixa temperatura de homogeneização e baixa salinidade, sugerindo uma mistura de fluidos magmáticos e meteóricos para a precipitação dos minerais de minério. Além disso, a baixa temperatura de homogeneização da cassiterita ajudou a compreender os principais mecanismos de incorporação de índio e metais raros.
- Adicionalmente aos dados de inclusões fluidas, os minerais do grudo da helvita trazem informações sobre o fluido mineralizante. A predominância de danalita sobre helvita e genthelvite sugere uma maior disponibilidade de Fe no sistema. Como esse mineral é estável em um domínio restrito de fugacidade de oxigênio e enxofre (domínio de estabilidade da pirrotita; Fig.12), conclui-se que a formação das zonas mineralizadas ocorreu preferencialmente sobre as mesmas condições de fugacidade de oxigênio e enxofre.

- Os dados de isótopos de enxofre apresentam valores de $\delta^{34}S$ entre -4.86 a -1.52 ‰, o que se assemelham a $\delta^{34}S$ derivado de uma fonte magmática. Dessa forma, o magma granítico representa uma provável fonte para o enxofre do sistema hidrotermal no Maciço Sucuri. Esta assinatura do enxofre se assemelha àquela encontrada no depósito

de Sn-In do Maciço Mangabeira, já bem conhecido na Província e a vários depósitos de índio e estanho do mundo.

- Os resultados apresentados juntamente com os dados da literatura suportam a existência de dois episódios de mineralização de estanho (com índio associado) na Província Estanífera de Goiás. O primeiro está relacionado à suíte granítica g1 e o segundo, o mais estudado e mais importante, relacionado à suíte granítica g2.
- A mineralização relacionada a suíte g1, como a do Maciço Sucuri, é pouco expressiva e formada a partir de fluidos rico em flúor exsolvidos de um magma pouco evoluído. A formação da cassiterita ocorreu devido a mistura desse fluido magmático-hidrotermal com fluidos meteóricos. Tal processo resultou em fluidos puramente aquosos, de baixa salinidade e de baixa temperatura (<200ºC). Por ter se formado a partir de um magma pouco fracionado (em relação a suíte g2), a concentração de estanho e índio foi pouco efetiva não gerando altas concentrações de índio como observado nos outros depósitos da suíte. O contrário ocorre nos depósitos relacionados a suíte g2, como Mangabeira e Pedra Branca, formados a partir de fluidos aquo-carbônico (H_2O–NaCl–KCl–CO_2), com temperaturas acima de 300 ºC, derivados de rochas altamente fracionadas, como topázio albita granito.
- Os dados desse trabalho indicam que o Maciço Sucuri constitui um alvo com baixo potencial para um depósito expressivo de estanho e índio. Entretanto, devido a sua proximidade com o Maciço Mangabeira (~10 km, ambos situados às margens de rodovia asfaltada), poderia constituir uma fonte adicional de minério para uma exploração conjunta.